2013-06-19

Spectroscopic Investigation of Intra- and Intermolecular Interactions of Donor-Acceptor Pi-Systems

Edward Adjaye-Mensah
University of Miami, e.adjayemensah@umiami.edu

UNIVERSITY OF MIAMI

SPECTROSCOPIC INVESTIGATION OF INTRA- AND INTERMOLECULAR INTERACTIONS OF DONOR-ACCEPTOR PI-SYSTEMS

By

Edward Adjaye-Mensah

A DISSERTATION

Submitted to the Faculty
of the University of Miami
in partial fulfillment of the requirements for
the degree of Doctor of Philosophy

Coral Gables, Florida

June 2013

UNIVERSITY OF MIAMI

A dissertation submitted in partial fulfillment of
the requirements for the degree of
Doctor of Philosophy

SPECTROSCOPIC INVESTIGATION OF INTRA- AND INTERMOLECULAR INTERACTIONS OF DONOR-ACCEPTOR PI-SYSTEMS

Edward Adjaye-Mensah

Approved:

_____
James N. Wilson, Ph.D.
Professor of Chemistry

_____
M. Brian Blake, Ph.D.
Dean of the Graduate School

_____
Françisco M. Raymo, Ph.D.
Professor of Chemistry

_____
Norito Takenaka, Ph.D.
Professor of Chemistry

_____
Jaroslava Miksovska, Ph.D.
Professor of Biochemistry and Biophysics
Florida International University

ADJAYE-MENSAH, EDWARD (Ph.D., Chemistry)

Spectroscopic Investigation of Intra- and Intermolecular Interactions of Donor-Acceptor Pi-Systems (June 2013)

Abstract of a dissertation at the University of Miami.

Dissertation supervised by Professor James N. Wilson.
No. of pages in text. (80)

The use of fluorophores for specific applications is determined to a large extent by their optical and electronic properties. These properties, however, are controlled by their sensitivity to microenvironment as well as their intra- and intermolecular interactions. This research effort explores how molecular interactions affect the optoelectronic properties of selected fluorophores and, thus, guides their use as fluorescent probes or photoactive materials in organic electronic applications.

A combined spectroscopic and computational approaches was utilized in the first part to examine the photophysical properties of two different classes of probes: the highly responsive multisensing 4,6-diphenylpyrimidones and 4-[2-(6-hydroxy-2-naphthalenyl)-ethenyl]-1-methyl-pyridinium (**HNEP**$^+$) and its deprotonated form (**NEP**), a benzo-fused derivative of Brooker's merocyanine (**BM**). Our data indicate that the emission of the diphenylpyrimidones can be controlled by the identity of the electron-donating auxochrome, protonation state, solvent viscosity and polarity. Our investigation of **HNEP**$^+$/**NEP** establishes that **HNEP**$^+$/**NEP** and **BMH**$^+$/**BM** differ in the extent of charge delocalization in the ground and the excited states inspite of their similar pKa values and structural homology. **HNEP**$^+$ shows larger Stokes shifts compare to **BMH**$^+$ and **NEP** exhibits relatively enhanced solvatochromism to **BM**.

In the second part, we assess the relative contributions of geometric size, energy gap and frontier molecular orbital (FMO) features to π–stacking interactions in a series of donor-acceptor molecular constructs. These factors were correlated with the magnitude of charge-transfer association constants determined through spectroscopic (^{1}H NMR, UV-visible and steady state fluorescence) techniques. The results demonstrate that high molar absorptivity enhanced high charge transfer (CT) formation, while the energy difference between the HOMO-LUMO, π-surface area, symmetry, shape and size of FMO dictate the molecular orientations or ordering and hence the strength of CT complex formation. These studies provide insight into photophysical behavior of these fluorophores and how they can be used as probes or sensors or photoactive materials.

“The task is not so much to see what no one has yet seen; but to think what nobody has yet thought, about that which everybody sees" - Erwin Schrödinger

To

All the good people of this world

ACKNOWLEDGEMENTS

I gratefully thank Dr. James N. Wilson for his teachings, guidance, knowledge and kindness during my studies in his research group. I would like to express my sincere gratitude to Dr. Françisco M. Raymo and Dr. Norito Takenaka for their outstanding expertise and invaluable contributions that have shaped this research to this far.

I am thankful to Dr. Jaroslava Miksovska for her important collaboration, which lead to immense success of my research. I also take this opportunity to sincerely thank Walter G. Gonzalez who assisted me in her lab whenever I was there to work. Special thanks to Dr. Françisco M. Raymo again for opening his doors to me whenever the need arises to use his spectroscopic equipment, not forgetting Stefania Impellizzeri and Janet Cusido who were there to help on several occasions.

My appreciation goes to Dr. Burjor Captain for his contributions to the crystallography studies. My special thanks to Dr. Douglas Heller for his invaluable advice, suggestions and assistance. I am very grateful to Dr. Adam Braunschweig, whose strategic advice and suggestions brought a new inspiration to my life.

I am very grateful to Mr. Edward Torres and Dr. David Hudson for the great assistance I received from them during my studies in the Chemistry Department. I would like to express my appreciation to Sara Sucklal, Lydia Gonzalez, Susana Gadanyi and Raul Hernandez for their help and fruitful conversations that kept life going for me in Miami.

Many thanks to Erika Smith, Dr. Saleesh Kumar, Jyothi Dhuguru and Demar Pitter for all forms of contributions they made to my studies as labmates.

TABLE OF CONTENTS

LIST OF FIGURES

LIST OF TABLES

LIST OF SCHEMES

CHAPTER 1

Introduction

1.1 Overview and Applications of Conjugated Molecules

The development of fluorescent-based molecules has provided versatile and sensitive tools that serve as probes, imaging agents and sensors to investigate biomolecules, cells, organisms and organo-electronic devices.[1,2,3] The value of fluorophores stem from their optical and electronic properties and how to channel these characteristics to meet specific application. These properties however, are influenced by their response to microenvironment as well as their intra- and inter- molecular interactions. Some of the interactions found among conjugated molecules include hydrogen bonding, electrostatic, hydrophobic, Van der Waal forces, and π-stacking interactions.[4] The interactions of chromophoric molecules with their surroundings usually produce a chemical signal that is readily transformed into easily measurable electrical or optical event. The event may be fluorescent enhancement (turn-on) or quenching/attenuation (turn-off) which has unveiled outer and inner working of biological macromolecules including cell surface, cell membrane, proteins and nucleic acids.[1] π-stacking interactions play invaluable role in many areas including molecular recognition, intercalation of drugs in DNA and base stacking of DNA nucleotide. These interactions are found in the packing of aromatic molecules in crystals, the tertiary structure of proteins and the conformational preferences and binding properties of polyaromatic macrocycles and porphyrin aggregation.[5]

This work is divided into two segments with common focus on molecular interactions. The first part of this research examines the photophysical properties of two

different classes of probes. The highly responsive multisensing 4,6-diphenylpyrimidone probes that have found applications as nucleoside analogs and metal ion sensors and environmentally responsive probe, stilbazolium dye that serves as photoactive materials in nonlinear optical applications. The second part of the work focus on the synthesis, characterization of polycyclic aromatic molecules (PAMs) and subsequent assessment of charge-transfer complexes generated by π-stacking interactions between donor-acceptor pairs of PAMs.

1.2 Conjugated and Aromatic Molecules

Conjugated molecules can broadly be defined as an ensemble of atoms whose p-orbitals overlap. In conjugated systems single bonds alternate with double bonds in cyclic, acyclic, linear or mixed connection of atoms. Aromatic molecules are conjugated molecules with one or more rings fused together in planar form to confer extra stability. The π-electrons in an align and close π-orbitals between atoms are much more mobile with low potential energy barrier due to conjugation than σ electrons.[6] Examples of conjugated molecules are shown in Figure 1.0.

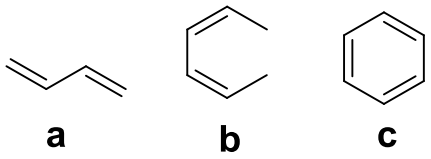

Figure 1.0 Conjugated molecules: (a) 1,3-butadiene (b) 2,4-hexadiene (c) benzene.

The most interesting electronic features of conjugated molecules include their ability to absorb and emit light, formation and transport of charge, as well as capability to accept or donate one or more electrons under illumination render them useful as semiconductors.[3, 6,7] Polymers of conjugated organic molecules have offered possibilities of obtaining cheap and easy methods to produce energy from light. The chemical

structures of the polymers can be manipulated to tune their optical properties for desirable applications. Organic semiconducting molecules/polymers can be synthesized at low cost and processed in either solution or vacuum evaporation/sublimation.[8] Thus, their optoelectronic properties coupled with easy processing techniques make conjugated molecules attractive and suitable for organoelectronic devices such as organo photovoltaic, light emitting diodes, and optical switches.[9]

1.3 Optical Processes or Mechanisms in Conjugated Molecules

Dyes and pigments appeared colored due to absorption of electromagnetic energy by the compounds within the visible region (400-700 nm), which is detectable by the human eye. The moiety within the molecule which absorbs light, resulting in electron excitation and emission of photon of a specific color in the visible spectrum is the chromophore. The chromophore usually contains conjugated systems bearing simple unsaturated groups such as $-NO_2$, -N=N-, -C=O. Auxochromes are either electron donators or acceptors tethered to a chromophore. They alter and shift the absorption wavelength of chromogens into the visible region by extending the conjugation. Fluorophores are molecules which can absorb photon of specific wavelength in the U.V. region and emit it at a different wavelength (usually at lower energy).

When an electron in a fluorescence molecule is excited by light from the singlet ground state to singlet excited state, it can undergo relaxation through radiation and radiationless decay pathways. The later pathway results when the electron relaxes to a singlet ground state via vibrational deactivation. The internal conversion is a typical radiationless decay process, which occurs from relaxation of electron in higher to lower ($\nu = 0$) vibrational energy levels in its excited state. Similarly, intersystem crossing

occurs when an electron relaxes from singlet excited state to triplet excited state. An electron in the excited state may relaxes through common radiation or emission pathways namely fluorescence and phosphorescence. Phosphorescence involves relaxation of an electron from singlet triplet state to ground state whereas fluorescence occurs when an electron relaxes from the singlet excited state.

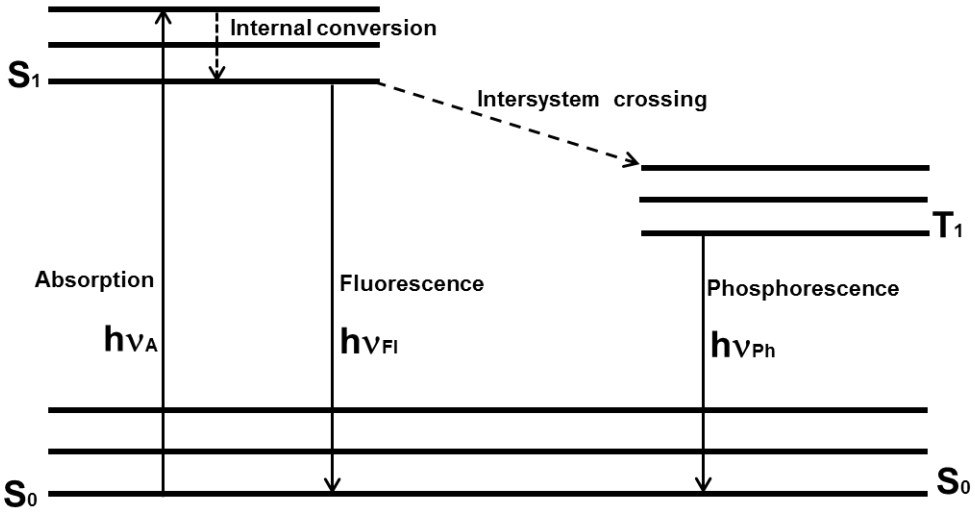

Figure 1.1 Simplified Jabloski energy diagram for organic fluorophore.[10]

The intensity, energy and lifetime of fluorescence of a molecule in the excited state are dictated by the microenvironment and the structure of the molecule.[10] Conjugated molecules display large change in dipole moment on excitation in solvents of different polarities. If the dipole moment of the excited state molecule is greater than that of its ground state (Figure 1.6), solvation by solvent molecules of increasing polarity can lower the energy (stabilize) of the excited state prior to emission to exhibit positive solvatochromism and vice versa.[1] The strong response of fluorophores to solvent polarity is used to estimate local polarity in membranes, proteins and DNA. Tryptophan is typical of such class of fluorophores, which in addition can be affected by quenchers such as

disulfide bonds, protonated histidines, metal ions, peptide bonds, coenzymes and heme groups.

Certain family of chromophoric probes have low quantum yield in non-viscous media due to rotational relaxation about the single bond joining the two π systems, as the major nonradiative decay pathway. In viscous media their structural rigidity is enhanced by reduced rotation and hence increased in their quantum yield. The twisted intramolecular charge transfer (TICT) excited singlet state of these chromophores has been used to investigate microviscosity and fluidity of membranes. Example is 4-(dicyanovinyl)julolidine.[1]

1.4 Applications of Fluorescence Signaling

Fluorescence of molecules is widely applied in biological imaging and sensing.[11] Although, numerous applications of fluorophores have been reported, their utility often depends on how their optical properties can be modulated to meet specific needs. The optical response and hence, their utility are largely determined by their structural motifs and sensitivity to their microenvironment such as solvent, protonation, polarity, viscosity, presence of quenchers and solid state. Molecular probes for imaging in cell biology can be highly fluorescent than the specimen's constituents, hence their presence and location in living cells can be monitored with spatial and temporal resolution.[12]

Fluorescence quenching has been employed to study a number of systems including RNA folding dynamics, charge-transfer complexes, dynamic and conformational properties of proteins and microdomains in membranes.[13] The emission intensity of fluorophore (usually a donor molecule) is attenuated in the presence of a quencher (usually an acceptor molecule).

Decorated porphyrins were used as optical sensors for saccharides. The advancement in the design of fluorophores attached to boronic acids that have high tendency to form five or six membered cyclic esters with 1,2 or 1,3 diols respectively, have generated many carbohydrate sensors and receptors. Boronic acids sensors include derivative of stilbenes, N-phenylnaphthalimide and naphthalene.[1]

The visible fluorescence of the green fluorescent protein (GFP) has been utilized for noninvasive live cell imaging. GFP a member of the fluorescent proteins (FPs) fluoresces alone or in genetic fusions with other proteins. Mutagenesis of FPs can either lead to increase photostability or formation of reversible or irreversible photoswitchable FPs that change from one color to another or display "OFF / ON" effect. The photoswitching behavior of FPs is harness to monitor protein diffusion, trafficking and age.[2]

Fluorescence nucleoside capable of sensing more than one environmental parameter with a unique spectroscopic signature is used for probing nucleic acid recognition, dynamics and damage.[14]

Expanded or extended nucleobases are utilized to monitor oligonucleotide denaturation, explore size-expanded DNAs, base-discriminating fluorescent nucleoside for single nucleotide polymorphism detection, tools to evaluate electron transfer processes in DNA, detecting DNA and RNA lesions.[1]

The fluorescence of carbohydrate-functionalized conjugated polymers have allowed versatile and quick method to detect range of pathogens such as bacterial.[15]

Near infrared fluorescent probes that turn-on upon binding with amyloid-beta (Aβ) peptide have been developed to improve imaging and detection of amyloid.[16]

Fluorescent conjugate polymers have found diverse applications as sensors for ions, metal ions, small biomolecules, detectors for explosives, DNA, etc. [13]

1.5 Interactions of Conjugated Molecules

Conjugated molecules have unique electronic structure that facilitates intramolecular interactions or intermolecular interactions or interact with their surroundings. These interactions to a larger extent control the optoelectronic properties of conjugated molecules for specific application.

1.6 Molecule-Molecule Interactions

π-stacking interactions are commonly encountered in conjugated aromatic molecules. Stefan Grimme and C.A. Hunter definitions for π–π interactions are adopted for purpose of this report. Grimme defined π–π interactions as nonlocalized, noncovalent, interactions between unsaturated organic groups, which are spatially closed in a stacked orientation.[17] Hunter on the other hand described aromatic rings as positively charged σ-framework sandwiched between two regions of negatively charged π-electron density. Hunter's definition described π–π interactions as attractive interactions between the π-electrons and the σ-framework, which outweighs the unfavorable π-electron repulsion contributions.[5,18] In general π-stacking interactions are combination of electrostatics, induction, dispersion and repulsion energies between conjugated molecules in a stacked orientation. Aromatic building blocks can interact in different orientations including *edge-to-face* used to describe the favorable T-shaped, perpendicular arrangement of aromatic rings, *stacked* describes the non-favorable parallel arrangement and *offset stacked* describes the favorable parallel arrangement (Figure 1.2)

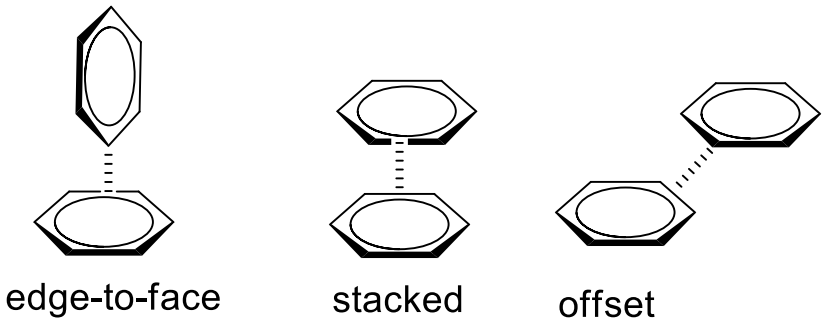

Figure 1.2 Different orientations of benzene dimer.

Excimers are transient excited state dimers formed by association of excited and unexcited molecules (monomers), which dissociate in the ground state. The fluorescence excimer of many aromatic molecules in a higher concentration and in crystalline state is distinct by the formation of broad and structureless emission band at longer wavelengths.[19]

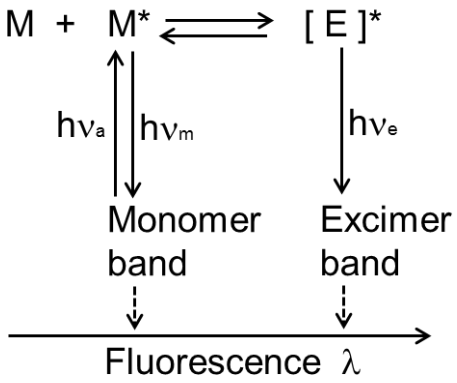

Figure 1.3 Excimer formations by aromatic molecules.

Photon absorption by donor molecule generates singlet exciton; hole-electron pair held by coulombic attraction. At the interface with acceptor molecule, the exciton may dissociate either by the offset between donor's highest occupied molecular orbital (HOMO) and acceptor's lowest unoccupied molecular orbital (LUMO) or external field such that holes are localized on HOMO and electrons on the LUMO. If the coulombic

attraction is sufficiently significant, the dissociation does not result in free charges but bound electron-hole pair or charge transfer (CT) exciton. The CT state is intermediate between a fully dissociated charges and excitons. The lowest and highest energy CT state are also referred to as exciplex and geminate respectively.[20, 21, 22] CT state are evidenced by the presence of weak optical absorption and (electro) luminescence bands. Molecular complexes in which CT state are formed are called CT complexes. Aromatic donor and acceptor molecules with well-defined optical and electronic properties can be assembled to form charge-transfer (CT) complexes. Formation of a CT complex is a consequence of intermolecular coupling and thus, an effective tool to modulate optoelectronic properties of polycyclic aromatic molecules (PAMs) geared toward organic electronics applications.[5]

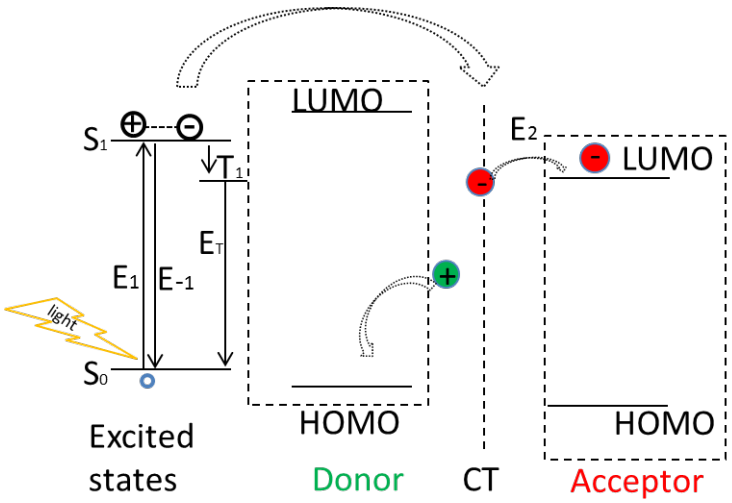

Figure 1.4 Illustration of exciton and charge transfer state in donor-acceptor system.

The strong Van der Waal's attractive forces in conjugated molecules generally enable them to self-aggregate in solution or at solid-liquid interface. These strong electronic interactions generally lead to self-quenching. The aggregated molecules

possessed distinct absorption band from their monomeric species. The distinct optical responses of bathochromic shifted J- [23, 24] and hypsochromic shifted H-[25] aggregates have served as important tools to study bonding and intermolecular interactions. Most chromophores aggregate in the solid state or films with reduced quantum yields known as aggregation caused emission quenching (ACQ). On other hand, some chromophores have been reported to exhibit aggregation-induced emission (AIE) of high quantum yield (QY) in thin solid films or poor solvents. Pasini and co-workers reported push-pull chromophore, which has bright emission in the solid state solution due to restricted intramolecular rotation and formation of dimeric J-aggregate but almost quenched in solution. Extending the π-framework of the chromophore yielded two compounds with high QYs resulting from reduced rotation in solution and quenched in the solid by strong intermolecular interactions.[26] Quenching is the loss of fluorescence intensity of a molecule in the presence of a quencher usually in the form of ions or metal ions or solvent molecules or another molecule (Figure 1.5). Fluorescence quenching by a quencher commonly occur by dynamic (collisional) and static (associated complex) processes.[1, 13]

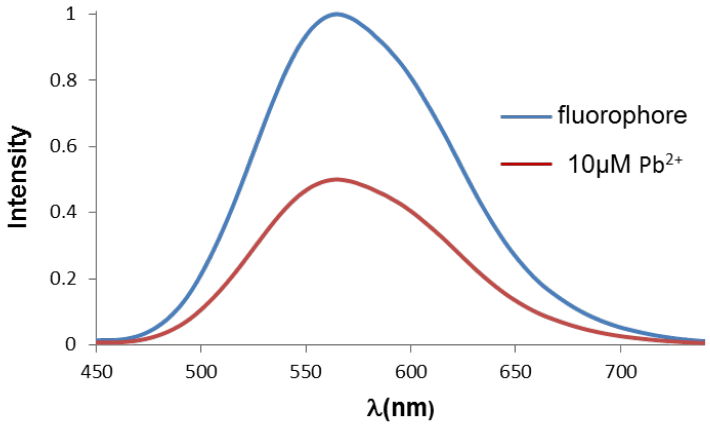

Figure 1.5 Spectrum illustrating fluorescent quenching.

1.7 Solvent-Molecule Interactions

The response of fluorophores to their surrounding factors including solvent polarity, pH, viscosity, quenchers etc. usually induce either change in emission intensity or shifts in the spectra wavelength. The changes in their photophysical properties have provided a platform for them to be utilized as probes or sensors to explore biomolecules.[27] Solvents effect on spectra properties of molecules is termed as solvatochromism. The solvatochromism of molecules in solvent could generally be bathochromic (positive) or hypsochromic (negative) shifts and is used as simple indices to classify their environment.[28,29] Merocyanine dyes are typical molecules notable of solvatochromic behavior.[25]

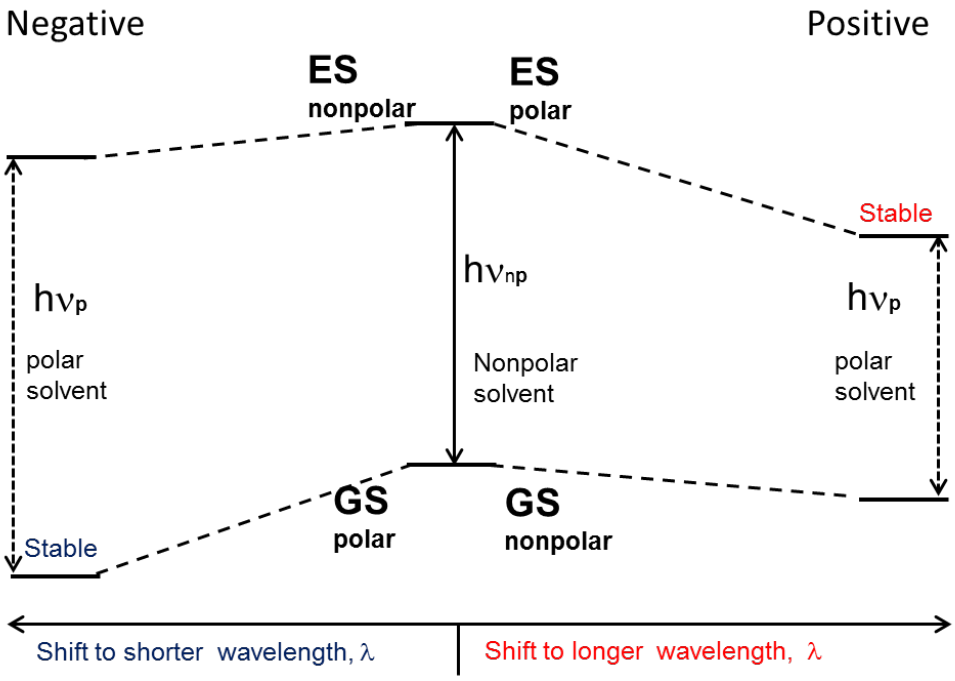

Figure 1.6 Solvatochromic behaviors of organic molecules in solvents.

Molecular probes have specific characteristics that make them interact and sense a small change in their microenvironment and hence show evidence of solvatochromism. Depending on the structure, the spectral of some molecules are sensitive to pH changes

which could stabilize or destabilize the molecules. Structural stability on protonation may possibly result from hydrogen bond formation that confers rigidity while destabilization may adversely alter its photophysical properties. Some chromophore display TICT in less viscous media thus, locking the molecular rotor in a more viscous media often lead to comparable structural rigidity and enhance optical characteristics. An emissive isomorphic pyrimidine containing multiple sensory elements to simultaneously probe polarity, acidity and viscosity with a distinct spectral signature for each environmental factor was reported by Tor and co-workers. The chromophore (Figure 1.7) shows reduced rotation in viscous media and formed intramolecular hydrogen bonding to extend the π-conjugation upon protonation, both of which promote planarization, thereby increasing fluorescence via reduced non-radiative relaxation pathway. The probe sensitive to polarity changes associated with changes in viscosity and acidity was also reflected by change in the stokes shift due to electronic polarization either in the ground or excited state.[14]

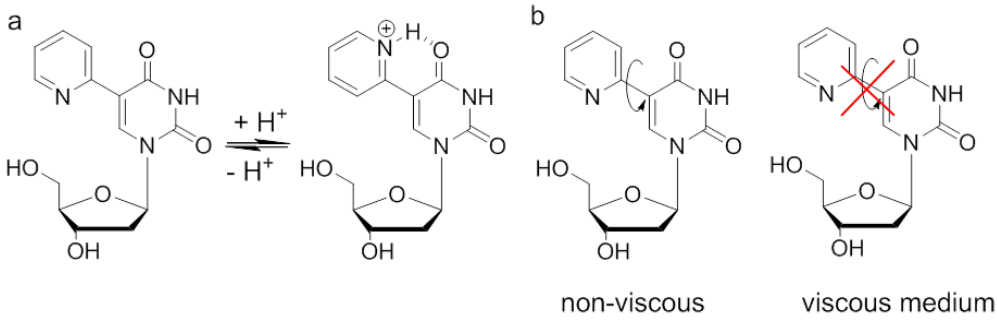

Figure 1.7 Structural consequences of isomorphic pyrimidine; (a) protonation results in H-bond formation to increase rigidity, (b) reduced rotation in viscous medium.[14]

1.8 Emission Switching of 4,6-Diphenylpyrimidones

The mechanisms of emission switching of 1-ethyl-4,6-bis(4-(dimethyl-amino)phenyl)-2(1H)-pyrimidone and 1-ethyl-4,6-bis(4-methoxyphenyl)-2(1H)-

pyrimidone in response to environment parameters such as protonation, solid state, solvent polarity and viscosity, their photophysical properties were investigated in chapter 2. The polarity dependence of the vertical excitation energies were unravel through UV-Vis and steady state emission spectroscopy of the protonated and unprotonated forms for a range of solvents. Emission lifetimes and quantum yields show the solvent dependency of the excited states. In polyethylene glycol solutions and in the solid state (both thin film and single crystal), their emission were enhanced, which showcase the role of intramolecular rotation in thermal relaxation of the excited states. TD-DFT calculations were used to provide insights into the excited state geometries and the role of intramolecular charge transfer. The results indicate that emission of diphenylpyrimidones can be altered by the identity of the electron-donating auxochrome, protonation state, solvent viscosity and polarity.

1.9 Photophysical Characterization of Stilbazolium Dye

The photophysics of 4-[2-(6-hydroxy-2-naphthalenyl)-ethenyl]-1-methyl-pyridinium (**HNEP**$^+$) and its deprotonated form (**NEP**), a benzofused derivative of Brooker's merocyanine (**BM**), were investigated in chapter 3 through spectroscopic and computational approaches. Although **HNEP**$^+$/**NEP** and **BMH**$^+$/**BM** have similar pKa values and structural similarities differ in the extent of charge delocalization in the ground and excited states. **NEP** exhibits the spectral characteristics of a charge transfer species in solvents in which **BM** exists in a charge-delocalized quinoid. However, quantum chemical calculations show that the CT absorption of **NEP** is not necessarily a consequence of the zwitterionic character. **HNEP**$^+$ displays larger Stokes shifts than

BMH^{+} and **NEP** demonstrates enhanced solvatochromism relative to **BM** as a consequence of benzofusion.

1.10 Assessing Charge Transfer Complexes using π-π interactions

We investigated the charge-transfer complexes formed by PAMs whose electronic and optical properties can be tuned without structural modification in chapter 4. Our primary focus was to assess relative contributions of geometric size, HOMO-LUMO energy gap and FMO features to π-stacking interactions in different molecular constructs. These factors were correlated with the magnitude of charge-transfer constants determined through spectroscopic (^{1}H NMR, UV-visible and steady state fluorescence) techniques. The results demonstrate that **PY-NDI** complex exhibits high CT formation at high energy (short wavelength) for all the spectroscopic methods used. Thus, peak out as potential molecules for single step electron transfer from the donor to acceptor. The role of molecular geometry and symmetry were clearly observed for **PY** and **CHR** versus **NDI**, while the effects donor's donating and acceptor's accepting abilities on the strength of CT is seen in the case of **PY** and **TPH** versus **NDI** and **MTI** in ^{1}H NMR studies. In addition to reinforcing the effects of geometry, symmetry and large π-surface area, the UV-visible experiments revealed the significance of molar absorptivity on forming strong CT complexes. Steady state emission and lifetime quenching of **PY** with **pNDI** (**25mer**) suggest that dynamic quenching becomes significant in polymer-monomer interaction at varying temperatures. Also, for each donor-acceptor pair investigated, it was apparent that energy gap between the $HOMO_D$-$LUMO_A$, π-surface area, FMO's symmetry, shape and size dictate the molecular orientations or ordering and hence the strength of CT complex formation.

1.11 Summary

This thesis focuses on the impact of microenvironment, intra- and intermolecular interactions on the photophysical properties of some selected fluorophores. The fluorophores considered here can be used as probes or as photoactive materials in organic electronic application, therefore this investigation with a variety of spectroscopic methods will shed light on how to modulate their optoelectronic behaviors to suit their intended applications.

CHAPTER 2

Emission Switching of 4,6-Diphenylpyrimidones: Solvent and Solid State Effects

2.1 Overview and Biological Significance of Pyrimidones

Pyrimidone is a widespread heterocyclic core whose derivatives form the basis of many biological molecules such as the nucleobases and barbiturates (Figure 2.0). It is found in many pharmacologically active compounds[30,31] and in nucleic acid chemistry.[32, 33] For instance, aryl-substituted pyrimidones have been analyzed as antimicrobials, kinase inhibitors, and analgesics.[34,35] The aryl pyrimidones are known to be optically active materials as a result of their structural motif. Their optical property makes them useful as fluorescent probes and guides the development of biologically pertinent fluorophores.

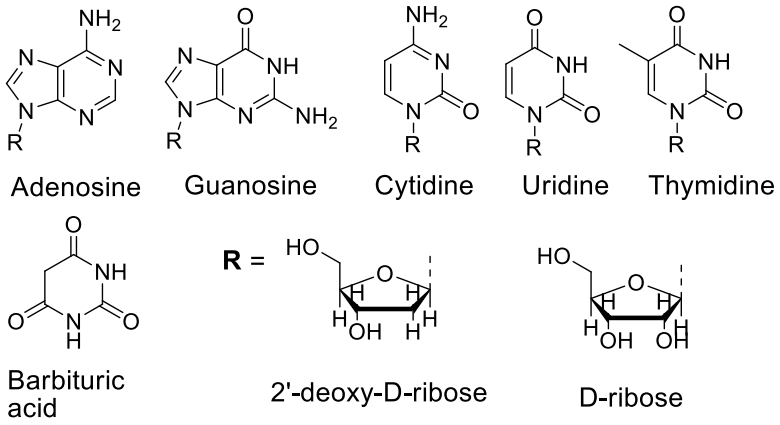

Figure 2.0 Structures of barbituric acid, ribo- and deoxyribonucleosides.

2.2 Definition and structure of arylpyrimidones

Aryl-substituted pyrimidones consist of hydrogen bonding pyrimidone moiety linked to hydrophobic aryl substituent. This structural design affords several modes of interaction in binding to bio-molecular target. The molecular architecture of diphenylpyrimidones in particular can be envisaged as a π-system of an electron withdrawing pyrimidone core with two pendant electron-donating phenyl arms. This

arrangement can be represented simply as a donor-acceptor-donor (D-A-D) π-system as shown in Figure 2.1.

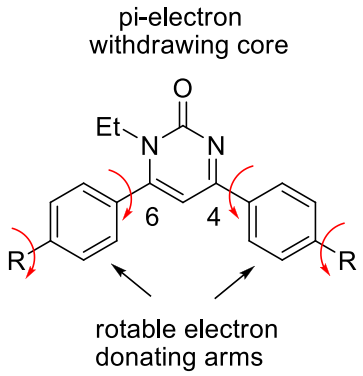

Figure 2.1 Donor-acceptor-donor π-system of diarylpyrimidone showing possible modes of rotation.

2.3 Pyrimidone fluorophores

Fluorescent pyrimidines are a class of highly responsive, multisensing probes[14] that have found applications as nucleoside analogs[36] and metal ion sensors.[37,38] The pyrimidine moiety alone exhibits optical transitions at relatively high energies. However, their absorption and emission can be tuned to more useful energies through structural modification by extension of conjugation and introduction of auxochromes. Extending the conjugation of the pyrimidine core can be accomplished via benzofusion or addition of a rotatable aryl group; examples of the former include the expanded nucleobases of Kool[39] and Moreau[40] whereas the latter are typified by the pyrimidine constructs reported by Tor[41] and others.[42,43] Despite the fact that aryl pyrimidones are important pharmacological molecules, only a few reports have examine their photophysical properties.[37,44] A series of phenylpyrimidones that exhibit large proton-induced enhancements in molar absorptivity (i.e. hyperchromicity) as well as substantial bathochromic shifts in their absorption maxima were reported by our group.[45] These

chromic shifts are coupled to changes in emission. We were enticed by the notable photophysical behavior of two constructs in the series, specifically, 1-ethyl-4,6-bis(4-(dimethyl-amino)phenyl)-2(1H)-pyrimidone(**1**) and 1-ethyl-4,6-bis(4-methoxyphenyl)-2(1H)-pyrimidone(**2**) (Figure 2.2).

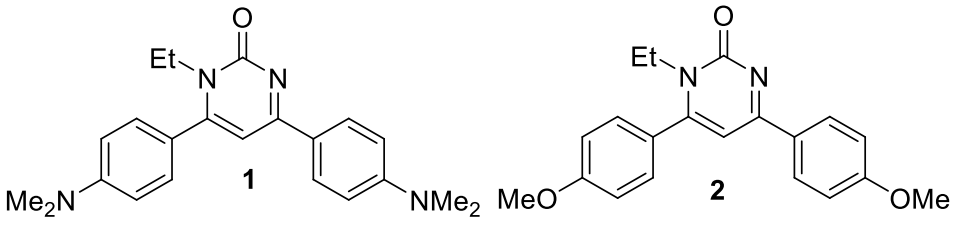

Figure 2.2 Chemical structure of specific 4,6-diphenylpyrimidones, **1** and **2** studied.

Though they are nearly identical in structure (differing only in the identity of the electron-donating auxochrome) and exhibit similar chromicity upon protonation, their emission response were found to be exactly opposite: while **1** is quenched in several organic solvents, **2** functions as a 'turn-on' probe when protonated. Although HOMO-LUMO gap and allowability of the vertical electronic transitions can be rational explanation of the chromicity of these fluorophores, their switchable emission currently cannot be warranted on the same premises. In this chapter we tasked ourselves mainly to understand the contrasting emission response (ON-OFF vs OFF-ON) of **1** and **2** at the molecular level, and more generally how to integrate these responses into functional fluorescent probes base on structural framework.

2.4 Solvent and protonation effect on the diphenylpyrimidones

The absorption and emission spectra of **1** and **2** were measured for the neutral and protonated ($\mathbf{1H^+}$ and $\mathbf{2H^+}$) forms in solvents of varying polarities. These solvents include methanol, ethanol, 2-propanol, acetonitrile, dimethyl sulfoxide, dimethyl formamide,

acetone, dichlromethane, chloroform, ethylacetate, tetrahydrofuran, toluene, cyclohexane, hexane and polyethyleneglycol. We focus initially on the two highly emissive species, neutral form of **1** and the protonated form of **2** (**2H**$^+$), by examining their ground and excited states across a range of solvents utilizing UV-vis spectroscopy, steady-state fluorescence spectroscopy and fluorescence lifetime measurements. The absorbance and emission spectra of **1** and **2H**$^+$ in cyclohexane, toluene, chloroform, acetone, isopropanol, ethanol and methanol are shown in Figure 2.3.

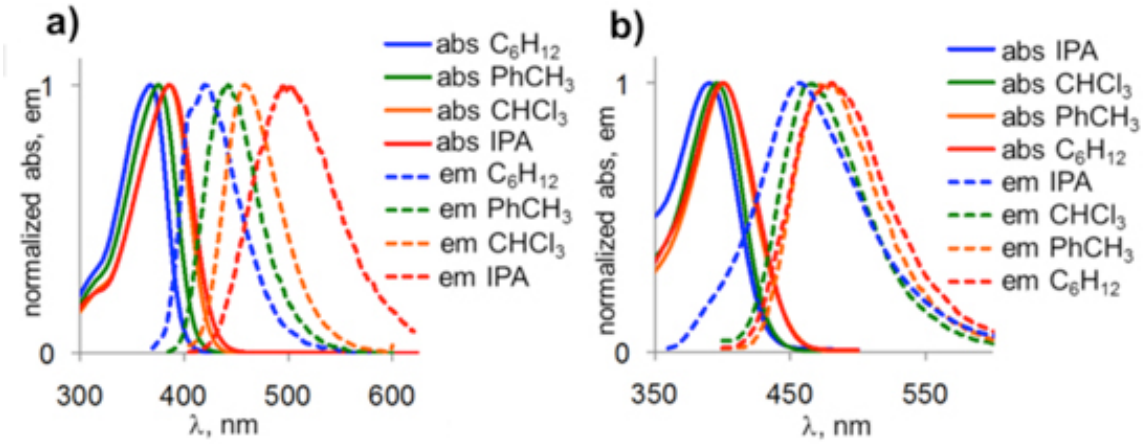

Figure 2.3 Absorption and emission spectra of (a) **1** exhibiting positive solvatochromism (b) **2H**$^+$ exhibiting negative solvatochromism in selected solvents.

Several key differences were noted for **1** and **2** through solvent dependent optical spectra in-spite of their structural similarity. The solvatochromism observed in the absorption spectra suggests that **1** has a relatively polar, intramolecular charge transfer (ICT) -like excited state, while emission from **2H**$^+$ is the result of less polar excited state.

Table 2.1 Photophysical properties of **1**, **1H**$^+$, **2** and **2H**$^+$.

cpd	parameter	C_6H_{12}	$PhCH_3$	$CHCl_3$	acetone	2-propanol	EtOH	MeOH	PEG	film
1	$\lambda_{max,abs}$ (nm)	371	378	384	379	387	391	395	393	399
	$\lambda_{max,em}$ (nm)	419	444	457	491	501	514	507	504	508
	Stokes shift (cm^{-1})	3090	3930	4160	6020	5880	6120	5590	5600	5380
	ϕ_{em}	0.03	0.20	0.40	0.35	0.28	0.05	10^{-3}	0.22	-
	τ_{avg} (ns)	1.69	2.9	4.31	3.5	4.28	4.17	-	0.76	-
	τ_1(ns)	0.25	0.18	0.18	0.26	0.21	0.15	-	0.58	-
	α_1	0.38	0.32	0.25	0.48	0.41	0.60	-	0.94	-
	τ_2 (ns)	2.51	2.92	2.79	2.83	2.86	2.89	-	3.91	-
	α_2	0.41	0.40	0.45	0.27	0.28	0.18	-	0.05	-
	τ_3 (ns)	10	11.3	10.5	11.7	11.9	11.3	-	-	-
	α_3	0.20	0.26	0.28	0.23	0.29	0.20	-	-	-
1H$^+$	$\lambda_{max,abs}$ (nm)	495	494	494	494	498	494	490	504	473
	$\lambda_{max,em}$ (nm)	-	-	-	-	-	-	-	-	635
2	$\lambda_{max,abs}$ (nm)	339	340	336	339	335	335	337	304	340
	$\lambda_{max,em}$ (nm)	-	-	-	-	-	-	-	412	408
2H$^+$	$\lambda_{max,abs}$ (nm)	400	401	396	390	390	387	386	394	399
	$\lambda_{max,em}$ (nm)	482	477	463	461	457	451	-	465	495
	Stokes shift (cm^{-1})	4250	3970	3650	3950	3760	3670	-	3880	4860
	ϕ_{em}	0.43	0.41	0.44	0.01	0.07	0.03	-	0.12	-
	τ_{avg} (ns)	2.73	1.82	1.58	1.51	0.88	0.69	-	0.986	-
	τ_1 (ns)	0.57	0.37	0.75	0.65	0.25	0.35	-	0.386	-
	α_1	0.25	0.31	0.57	0.79	0.44	0.79	-	0.358	-
	τ_2 (ns)	3.46	2.47	2.68	5.36	1.38	2.02	-	1.32	-
	α_2	0.75	0.69	0.43	0.19	0.56	0.20	-	0.644	-

2.4.1 Effects of protonation of 1 and 2 at the ground state

The absorption maxima obtained in cyclohexane, toluene, chloroform, acetone, isopropanol, ethanol and methanol are plotted as a function of $E_T(30)$ values in Figure 2.4.[46]

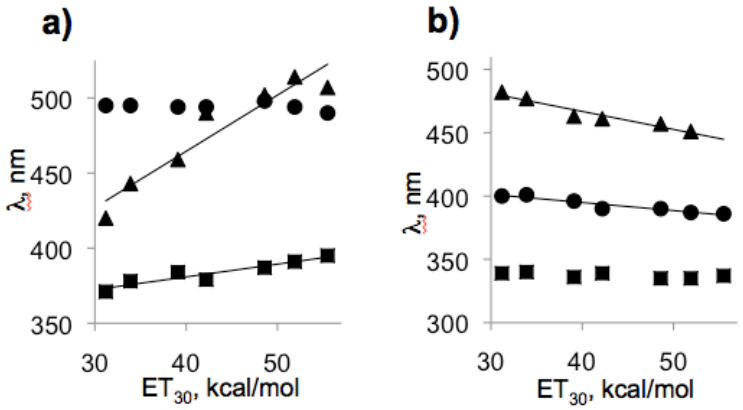

Figure 2.4 (a) Linear regression analysis of $\lambda_{max,\ abs}$ **(■)** and $\lambda_{max,\ em}$ **(▲)** of **1** correlates (R^2 = 0.90 and 0.91, respectively) with $E_T(30)$ values, while $\lambda_{max,\ abs}$ of $\mathbf{1H^+}$ **(●)** does not. (b) Linear regression analysis of the $\lambda_{max,\ abs}$ **(●)** and $\lambda_{max,\ em}$ **(▲)** of $\mathbf{2H^+}$ shows 1st order dependence (R^2 = 0.92 and 0.93, respectively) on solvent $E_T(30)$ values,[47] while $\lambda_{max,\ abs}$ of **2** **(■)** does not.

Pronounced solvatochromic effects were observed for **1** and $\mathbf{2H^+}$ while little or no solvatochromism was observed for $\mathbf{1H^+}$ and **2** (Figure 2.4). A positive solvatochromic effect was observed for **1** with an absorption maximum of 371 nm in cyclohexane, shifting to 395 nm in methanol. Positive solvatochromism implies that the excited state of **1** is more polar than the ground state. This is not unexpected considering the molecular architecture of **1** with strong electron-donating dimethylamino group coupled to an electron withdrawing pyrimidone core. This arrangement should contribute to an excited state with significant ICT-like character that would be stabilized in polar solvents such as methanol. $\mathbf{2H^+}$ displays negative solvatochromism, with an absorption maximum of 400 nm in cyclohexane, shifting to 386 nm in methanol. Negative solvatochromism indicates that ground state of $\mathbf{2H^+}$ is more polar than the excited state.[48] In a polar solvent such as methanol ($E_T(30)$ = 55.5 kcal/mol), the more ground state is stabilized than the excited state leading to a hypsochromic shift relative to cyclohexane ($E_T(30)$ = 31.2 kcal/mol). This effect is readily explained by the cationic nature of $\mathbf{2H^+}$, which should be stabilized

in a polar solvent. Photoexcitation may result in a redistribution of charge from the electron donating methoxyphenyl arms that leads to a less polar excited state. A comparison of the absorption spectra of **1** and $\mathbf{2H^+}$ shows that the energies of these electronic transitions are similar ranging from 3.1 eV to 3.3 eV for **1** and 3.1 eV to 3.2 eV for $\mathbf{2H^+}$. This is clearly demonstrated when **1** and $\mathbf{2H^+}$ are basically indistinguishable in chloroform solutions (Figure 2.5).

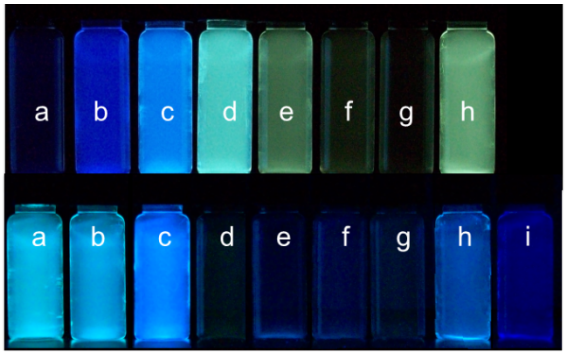

Figure 2.5 Photograph of illuminated (λ_{ex} = 354 nm) vials of **1** (top row) and $\mathbf{2H^+}$ (bottom row) evidencing solvent effect on $\lambda_{max,\ em}$ and Φ_{em}. (a) cyclohexane (b) toluene (c) $CHCl_3$ (d) acetone (e) isopropanol (f) ethanol (g) methanol (h) PEG. (i) Enhance Φ_{em} for unprotonated **2** in PEG.

2.4.2 Effects of protonation of 1 and 2 at the excited state

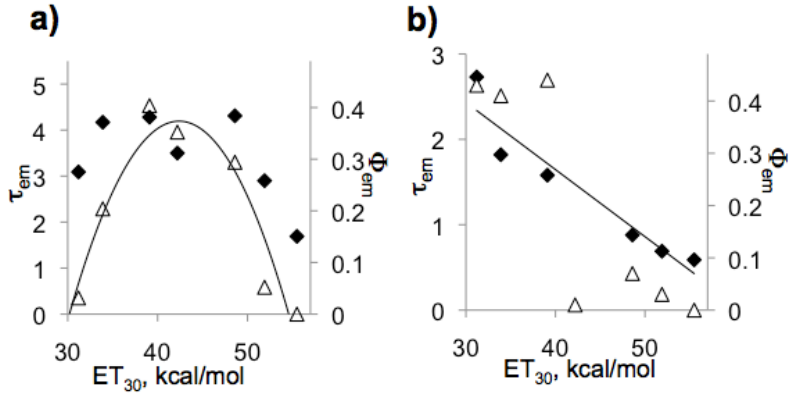

Figure 2.6 (a) Emission quantum yields of **1** (△) show a 2nd order dependence (R^2 = 0.90) on solvent polarity values and average emission lifetimes (◆) exhibit a similar effect. (b) Emission quantum yields of $\mathbf{2H^+}$ (△) are linked to solvent polarity and average emission lifetimes (◆) correlate well (R^2 = 0.91) with solvent polarity.

Next to examine is the emission spectra of **1** and $\mathbf{2H^+}$. The solvent-dependent emission spectra of **1** and $\mathbf{2H^+}$ follow the same trends observed in the absorption spectra; a positive shift in the case of **1** and a negative solvatochromic effect was found for $\mathbf{2H^+}$. For **1**, the effect was especially pronounced with a shift of 95 nm between cyclohexane ($\lambda_{max,\ em}$ = 419 nm) and methanol ($\lambda_{max,\ em}$ = 514 nm). This large bathochromic shift supports the notion that the emission of **1** is as a result of an ICT-like excited state. The hypsochromic shift found for $\mathbf{2H^+}$ was less pronounced with a difference of only 31 nm between cyclohexane ($\lambda_{max,\ em}$ = 482 nm) and methanol ($\lambda_{max,\ em}$ = 451 nm). The emission spectra and associated quantum yields provide further support for the view that **1** exhibits the strongest emission in moderately polar solvents while $\mathbf{2H^+}$ is emissive in less polar solvents. This trend is clearly vivid when comparing Figures 2.6a and 2.6b and in the photographs of illuminated solutions (Figure 2.5).

2.4.3 The identity of electron donating groups on aryl rotable arms

For most chromophore cores, inclusion of a dimethylamino substituent typically leads to lower energy optical transitions when compared to methoxy substitution.[49] With similar energies for **1** and $\mathbf{2H^+}$, it is likely that both methoxyphenyl arms of $\mathbf{2H^+}$ are conjugated through the pyrimidone core, thereby lowering the energy of the HOMO-LUMO transition, whereas only a single dimethylaminophenyl arm contributes in the case of **1**.

2.4.4 Effect of solvent polarity on quantum yields and emission lifetimes

Solvent polarity also influences the quantum yields of photoemission (Φ_{em}) and emission lifetimes (τ_{em}). Figures 2.6A and 2.6B show the effect of solvent on the emission intensity of **1** differs from that seen for $\mathbf{2H^+}$. The emission intensity of **1** peaks in moderately polar solvents such as chloroform and acetone with lower quantum yields

found in both cyclohexane and methanol or ethanol. As **1** was predicted to possess an excited state with ICT character, the quenching observed in the most polar solvents is expected, owing to strong solvent stabilization and subsequent thermal relaxation. The weak emission observed in cyclohexane (and to a lesser extent in toluene) may also be due to the ICT character of the excited state, which is poorly accommodated by less polar solvents. Emission lifetimes follow similar trend (Figure 2.6A) peaking in moderately polar solvents, $CHCl_3$ and isopropanol, with lower values in cyclohexane and higher polarity solvent such as ethanol and methanol.

While $\mathbf{2H^+}$ exhibits good quantum yields in relatively nonpolar solvents such as cyclohexane, toluene and chloroform with Φ_{em} ranging from 0.41 to 0.44, in polar solvents $\mathbf{2H^+}$ is only weakly emissive with a quantum yield of photoemission of 0.07 in isopropanol and emission was almost undetectable in methanol. The average emission lifetimes follow identical trends, ranging from 2.7 ns in cyclohexane to 0.7 ns in methanol.

2.4.5 Effect of solvent viscosity on the pendant rotable arms

The rotational freedom of both the phenyl arms as well as the dimethylamino auxochromes could contribute to energy losses that result in deexcitation. This effect has been noted in similarly constructed propeller-shaped fluorophores with rotatable arms. Reduction of rotation in the solid state leads to so-called aggregation-induced emission (AIE).[49] The rotational freedom of the pendant aryl groups is limited in solvents with greater viscosity. In solutions of polyethyleneglycol (PEG), the emission of **1** and $\mathbf{2H^+}$ was significantly enhanced relative to solvents with similar $E_T(30)$ values; quantum yields of photoemission in PEG are 0.22 for **1** and 0.11 for $\mathbf{2H^+}$. Contrast to non-emissive

behavior of **1H**$^+$ in PEG or in any other solvents considered, **2** shows clear evidence of emission (Figure 2.5) with emission maximum of 398 nm and a quantum yield of 0.04 in PEG though it is essentially non-emissive ($\Phi_{em} < 0.005$) in most solvents investigated.

2.5 Solid state Effect on the optical behavior of diarylpyrimidones

In the solid state, the rotation of the phenyl arms are predicted to be reduced and may lead to emission from **1H**$^+$ and **2**, which were not observed to be fluorescent in solution.[50]

2.5.1 Thin film studies on the optical response of diarylpyrimidones

Thin film absorption and emission spectra obtained for **1** and **2** in the neutral and protonated states are shown in Figure 2.7.

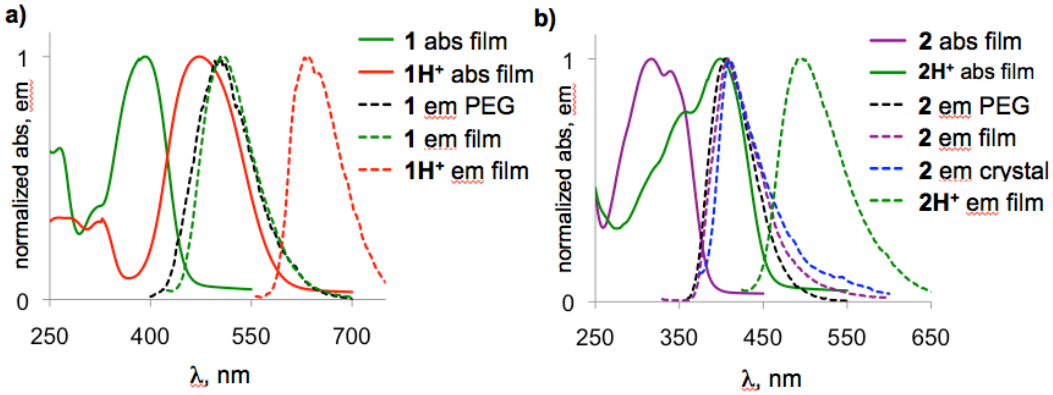

Figure 2.7 (a) Absorption and emission spectra of **1** and **1H**$^+$ in films with emission of PEG as reference. (b) Absorption and emission spectra of **2** and **2H**$^+$ in films, single crystal, and viscous PEG solutions. Emission of **2** is due to restricted rotation of the phenyl arms.

The thin film absorption spectra closely match those obtained in solution with the absorption maxima of the protonated forms bathochromically shifted relative to the neutral forms; this effect is clearly seen in Figure 2.8 as protonation of yellow films of **1** turn deep red while colorless **2** produces a yellow film.

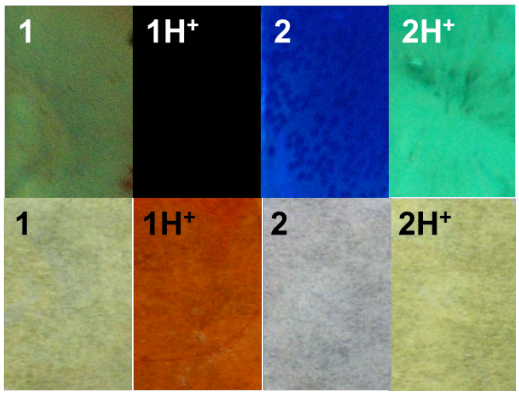

Figure 2.8 Photographs of UV illuminated (λ_{ex} = 354 nm) films (top row) and films under ambient light (bottom row).

Thin film emission of **1** also closely matches that observed in solution; it is also interesting to note that weak emission could as well be detected for the protonated form (**1H**$^+$), which was not observed in any solution measurements. The emission maximum is centered at about 635 nm, bathochromically shifted by approximately 125 nm relative to the neutral form. A similar shift is seen in the emission spectra of **2** and **2H**$^+$: the neutral form emits blue, whereas the protonated form emits green. The thin film emission observed for **2** is similar to that observed in PEG and reinforces the notion that quenching observed in most solutions is due to the rotational freedom of the pendant methoxyphenyl arms.

2.5.2 Crystallography studies on the optical response of diarylpyrimidones

Crystallographic analysis of **2** provides some insight into the molecular details that govern the optical properties (Figure 2.9) of this chromophore. The 4-(4-methoxyphenyl) arm is slightly twisted (7^o) relative to the pyrimidone core whereas the 6-(4-methoxyphenyl) arm shows a marked twist (52^o).

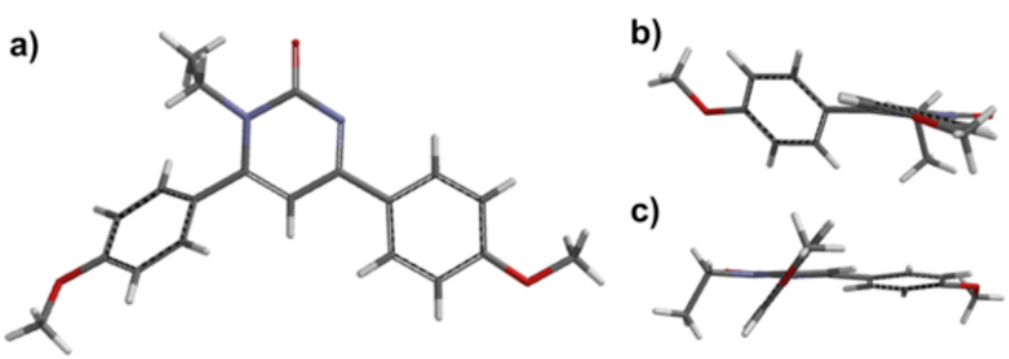

Figure 2.9 (a) The X-ray crystal structure of **2** shows (b) the 4-(4-methoxyphenyl) arm to be effectively coplanar with the pyrimidone core; twisted by an angle of 7° (c) the 6-(4-methoxyphenyl) arm is twisted 52°, effectively limiting π-conjugation with the pyrimidone core and opposite phenyl arm.

This suggests that only the 4-(4-methoxyphenyl) arm shares significant π-system overlap with the pyrimidone core and, as a consequence, the lowest energy optical transitions are likely localized to this conjugated donor-acceptor subunit. As the crystal emission spectrum correlates very well with spectra obtained from thin films and PEG solutions (Figure 2.6b), it appears that similar lumophores are present in all three cases. Thus, the quenching observed in solution is likely linked to rotation of the 4-methoxyphenyl arms. TD-DFT calculations (vide infra) provide further insight into the molecular orbital contributions to the photoluminescence and solvatochromicity of **1** and $\mathbf{2H}^+$.

2.6 Quantum chemical calculations on diarylpyrimidones

DFT and TD-DFT calculations reveal details of the structural and molecular orbital (MO) contributions to the electronic transitions observed in the absorption and emission spectra. The geometry of **2** obtained from the X-ray crystal structure was utilized as a starting point for all calculations. The ground state geometry of **2** calculated at the 6-31G* level in the gas and solution phases show very good agreement with geometry of the crystal structure. Small twist angles, ranging from 0.4° to 15°, are predicted between

the pyrimidone core and 4-(4-methoxyphenyl) arm, compared to 7° observed in the crystal structure; larger twists, ranging from 57° to 64°, are predicted for the 6-(4-methoxyphenyl) arm compared to 52° observed in the crystal structure.

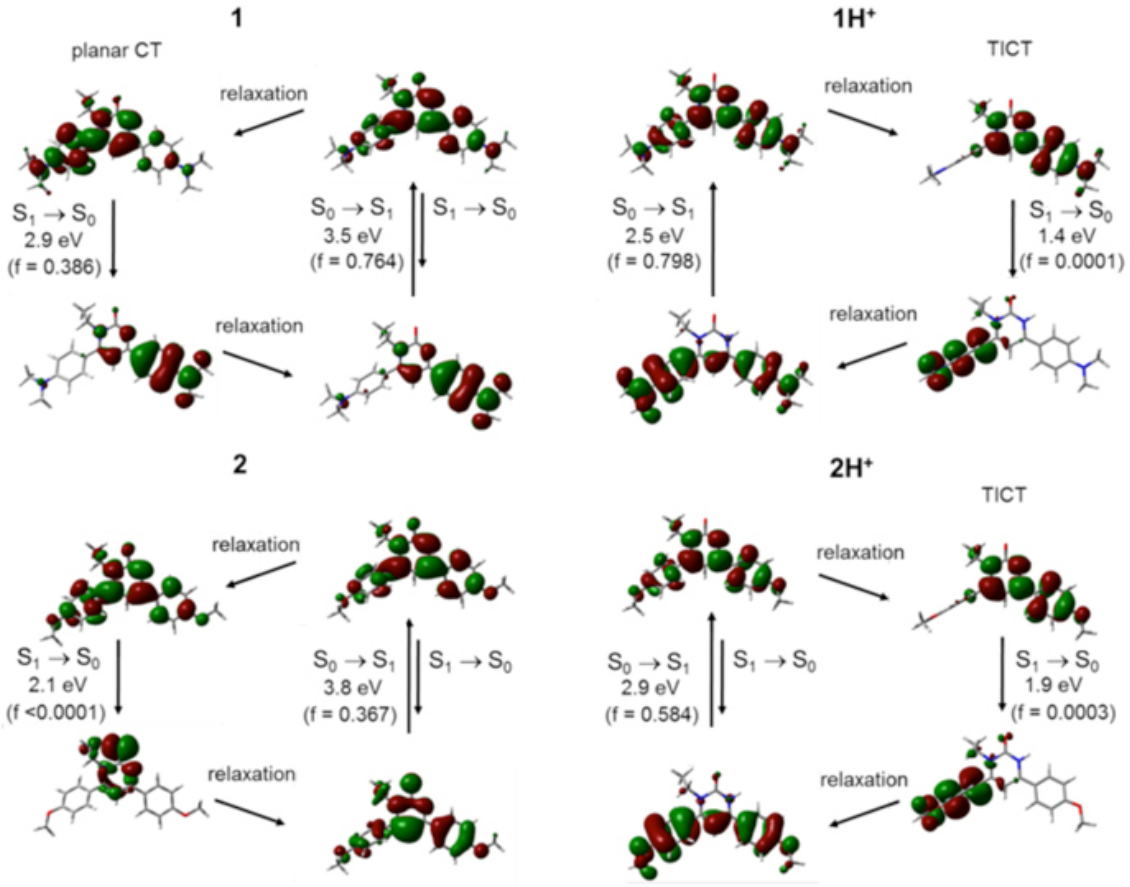

Figure 2.10 State energy diagrams, optimized geometries and contributing molecular orbitals for **1**, **1H**$^+$, **2**, and **2H**$^+$ obtained from DFT and TD-DFT calculations. HOMOs are mapped on the S_0 states while LUMOs are mapped on the corresponding S_1 states. Thermal relaxation following the vertical excitation produces non-emissive or 'dark' states for **1H**$^+$**, 2** and **2H**$^+$ with negligible oscillator strengths.

Figure 2.10 depicts the calculated transitions between the S_0 and S_1 states for **1**, **1H**$^+$, **2**, and **2H**$^+$ along with the relevant molecular orbitals, energies and oscillator strengths. Several aspects of these transitions correlate very well with the experimentally determined properties and provide further insights into the mechanisms of emission

switching. First, the calculated excitation energies are well matched with the experimentally determined values (Figure 2.11).

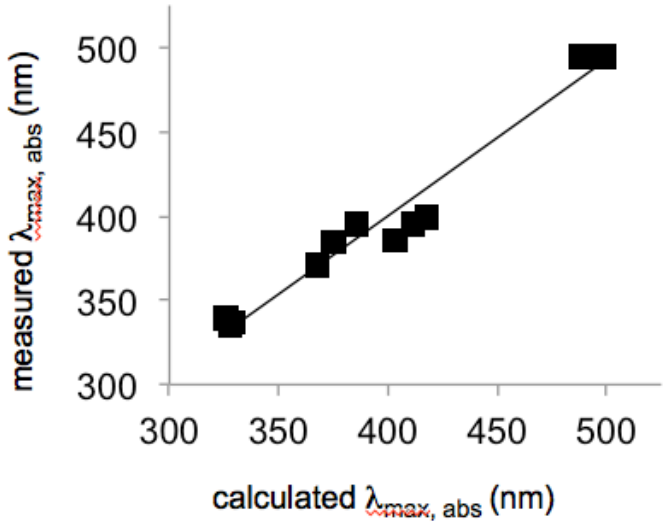

Figure 2.11 Calculated (TD-DFT, 6-31G*) absorption maxima correlate well ($R^2 = 0.97$) with observed absorption maxima in cyclohexane, chloroform and methanol.

The observed positive solvatochromic effect of **1** and negative solvatochromic effect of **2H**$^+$ are mirrored in the solvent-dependent TD-DFT calculations. Second, the solvent dependent chromicity suggested a more polar excited state for **1**. This is consistent with the highly localized molecular orbitals involved in the lowest energy electronic transition (Figure 2.10), which results in significant charge displacement producing a CT excited state. Finally, the TD-DFT optimized geometries also provide good qualitative agreement with the observed solvent dependent emission quenching.

One of the most striking features of these molecules is the contrasting emission response to protonation with **1H**$^+$ quenched in all solvents and thin films compared to **1** and **2H**$^+$ enhanced relative to **2** in most solvents. The quantum chemical calculations accurately account for this switching behavior and provide clear picture of the underlying mechanisms. Despite photoexcitation of **2** from the S_0 to S_1 state is predicted as an

allowed transition, twisting of the 4-methoxyphenyl arms produces a relaxed S_1 "dark state" as deduced from the low oscillator strength of the corresponding S_0 to S_1 transition in the gas phase, cyclohexane and chloroform. In methanol, significant oscillator strength (f = 0.65) is predicted for the lowest energy excited state conformation suggesting this state should be emissive, however, solution spectroscopy indicates that this is not the case. This difference may be attributed to the solvent model, which accounts for multipolar interactions but not hydrogen bonding interactions.

From the molecular orbital diagram it is clear that the allowed transition can be characterized as a π–π* transition in contrast to the n-π* transition for the non-emissive form. The rotation of the phenyl arm is reduced in PEG solutions, thin films and crystal forms which limits relaxation to the non-emissive S_1 state and dramatically enhances emission. $\mathbf{2H}^+$ exhibited strong emission in less polar solvents (e.g. Φ_{em} = 0.44 in cyclohexane) and significant quenching in polar solvents. Vertical excitation produces an excited state that is less polar than the ground state and is well accommodated in less polar solvents. However, the 6-(4-methoxyphenyl) arm of $\mathbf{2H}^+$ is also predicted to undergo rotation and thus, produce TICT-like "dark state" (f = 0.0003) that is likely responsible for the quenching observed in polar solvents. The enhancement observed in PEG and thin films reflect the reduced rotational freedom that largely minimizes energy lost via non-radiative pathway.

The emission of **1** was greatest in solvents of moderate polarity and was attenuated in the most polar and nonpolar solvents. Unlike **2** and $\mathbf{2H}^+$ where the excited state may relax to a non-emissive "dark-state", the thermally relaxed S_1 state of **1** is predicted to have significant oscillator strength. This is likely due to the greater electron-

donating ability of the dimethylamino group that enhances conjugation to the electron-withdrawing pyrimidone core. The more polar excited state predicted by both solution spectroscopy and quantum chemical calculations is probably poorly accommodated in less polar solvents leading to emission quenching. This is partially confirmed by the lower oscillator strength predicted by TD-DFT calculations in cyclohexane (f = 0.82) versus chloroform (f = 1.03). TD-DFT calculations also predict an emissive state in methanol, which is not supported by fluorescence spectroscopy, but may be due to hydrogen bonding not accounted for in the solvent model. The predicted geometries of the S_1 state differ only in the rotation of the 6-(4-dimethylaminophenyl) arm relative to the pyrimidone core. Thus, the observed emission enhancement in PEG is properly attributed to the reduced motion of the phenyl arm. It is interesting to note that the HOMO is largely localized to the 4-(4-dimethylamino-phenyl) arm. This is likely due to the strong electron donating ability of the dimethylamino group that is able to stabilize the electron-withdrawing pyrimidone core without the contribution of the 6-phenyl arm. This short conjugation length explains the relatively small difference in energies observed for the absorption and emission wavelengths of **1** versus $\mathbf{2H^+}$. In contrast, both **2** and $\mathbf{2H^+}$ see significant contributions to the HOMO from both phenyl arms. Protonation of **1** result in emission quenching that is readily explained by relaxation of the vertically excited S_1 state to a nonemissive TICT state. The spatially segregated molecular orbitals limit the strength of this transition ($f < 0.001$).

2.7 Conclusion

Our investigation into the emission switching of **1** and **2** reveals that rotation of the phenyl arms is the key factor in accessing relaxed, “dark” states by modulating

conjugation with the pyrimidone core. This is most clearly evident in the case of **2**, which is quenched in most solvents, but emissive in viscous solutions and the solid state. For the protonated species, $\mathbf{1H^+}$ and $\mathbf{2H^+}$, rotation of the 6-phenyl arm also results in a non-emissive TICT state as predicted by TD-DFT calculations. Solvent polarity also plays a role in emission switching through stabilization of the excited state as seen in the solvent dependent quantum yields of photoemission for both **1** and $\mathbf{2H^+}$. Finally, the strength of the electron-donating groups on the phenyl arms dictates the extent of the electronic interactions between the phenyl arms and pyrimidone core.

Our primary motivation was to explicate the contrasting emission response of **1** and **2** to protonation and it appears that this effect is limited to a narrow window of solvent polarities as the emission of $\mathbf{2H^+}$ is significantly quenched in solvents with $E_T(30)$ values above 41 $kcalmol^{-1}$. Understanding the molecular details governing switchable emission of arylpyrimidones serves to guide the development of fluorescent probes incorporating these structural motifs. Their polarity and viscosity sensitivity may be harnessed to generate fluorescent analogs of biologically relevant pyrimidines that report binding events, changes in biomacromolecular conformation or solvent interactions.

2.8 Experimental Methods

2.9 Steady-State Emission and Absorption Spectroscopy

Spectroscopy and HPLC grade solvents were utilized for all spectroscopic measurements; all path lengths were 1 cm. UV-vis absorption spectra were obtained on a Perkin-Elmer Lambda 35 UV-vis spectrometer using chromophore solutions of 10 μM to 20 μM. Trifluoroacetic acid (purity ≥ 98%) was used for the protonation of samples. Fluorescence studies were performed on a Perkin-Elmer LS55 Fluorometer. For

determination of Φ_{em}, solutions were prepared to an optical density of less than 0.05 in order to minimize inner filter effects. Perylene in cyclohexane was used as a reference for quantum yields.[51] Fluorescence lifetimes were obtained on a frequency-domain lifetime spectrometer ChronoFD from ISS exciting at 370 nm using POPOP or 1,4-bis(5-phenyloxazol-2-yl)benzene (scintillation grade) in ethanol as a standard.

2.10 Crystallographic Analysis

Colorless single crystals of **2** suitable for X-ray diffraction analyses were obtained by evaporation of solvent from a dichloromethane/methanol solvent mixture at 25 °C. The data crystal was glued onto the end of a thin glass fiber. X-ray intensity data were measured by using a Bruker SMART APEX2 CCD-based diffractometer using Mo Kα radiation (λ = 0.71073 Å).[52] The raw data frames were integrated with the SAINT+ program by using a narrow-frame integration algorithm.[52] Corrections for Lorentz and polarization effects were also applied with SAINT+. An empirical absorption correction based on the multiple measurement of equivalent reflections was applied using the program SADABS. The structure was solved by a combination of direct methods and difference Fourier syntheses, and refined by full-matrix least-squares on F^2, by using the SHELXTL software package.[53] Compound **2** crystallized in the monoclinic crystal system. The systematic absences in the intensity data were consistent with the unique space group $P2_1/c$. With Z = 8, there are two formula equivalents of **2** in the asymmetric crystal unit. All non-hydrogen atoms were refined with anisotropic displacement parameters. Hydrogen atoms were placed in geometrically idealized positions and included as standard riding atoms during the least-squares refinements.

Data collection parameters and results of crystal analysis are in Table 2.2.

Table 2.2 Crystallographic Data for **2**.

Empirical formula	$C_{20}H_{20}N_2O_3$
Formula weight	608.71
Crystal system	Monoclinic
Lattice parameters	
a (Å)	15.9181(7)
b (Å)	15.8933(7)
c (Å)	13.9220(6)
β (deg)	101.478(1)
V (Å^3)	3451.7(3)
Space group	$P2_1/c$ (# 14)
Z value	8
ρ_{calc} (g / cm^3)	1.295
μ (Mo Kα) (mm^{-1})	0.088
Temperature (K)	296
$2\Theta_{max}$ (°)	53.0
No. Obs. (I > 2σ(I))	5247
No. Parameters	458
Goodness of fit	1.014
Max. shift in cycle	0.001
Residuals*: R1; wR2	0.0393; 0.0985
Absorption Correction, max. / min.	Multi-scan 0.9930/0.9640
Largest peak in final diff. Map (e$^-$ / Å^3)	0.140

*$R = \Sigma_{hkl}(||F_{obs}| - |F_{calc}||)/\Sigma_{hkl}|F_{obs}|$; $R_w = [\Sigma_{hkl}w(|F_{obs}| - |F_{calc}|)^2/\Sigma_{hkl}wF_{obs}^2]^{1/2}$, $w = 1/\sigma^2(F_{obs})$; GOF = $[\Sigma_{hkl}w(|F_{obs}| - |F_{calc}|)^2/(n_{data} - n_{vari})]^{1/2}$.

2.11 Computational Analysis

All calculations were carried out utilizing the Gaussian '09 suite of electronic structure modeling software.[54] Ground state geometries were calculated by DFT with the B3LYP functional at the 6-31G* level in the gas phase and three solvents (cyclohexane, chloroform, and methanol).[47] Excited state geometries were optimized by TD-DFT at the 3-21G* level in the gas phase and the selected solvents. The atomic coordinates obtained from crystal structure of **2** were used as the starting geometries for the protonated and unprotonated forms of **1** and **2**. The vertical excitation energies were obtained from TD-

DFT calculations with B3LYP functional at the 6-31G* level. Molecular orbitals were visualized using the GaussView 5 program.

CHAPTER 3

Photophysical Characterization of a Benzo-fused Analogue of Brooker's Merocyanine: Solvent polarity and pH effects

3.1. Overview and Significance of Stilbazolium Dyes

Stilbazolium dyes are important substituted chromophores with attractive optical properties, which make them function as photoactive materials in nonlinear optical applications.[55,56] They have highly sensitive absorption and emission profiles that enable them useful as environmentally responsive probes.[57,58,59] Norepinephrine (NE) is a chemical messenger found in both the periphery and the central nervous system (CNS). In the CNS, NE plays key roles in regulating mood, stress responses, learning, memory and wake-sleep cycles.[60,61] The norepinephrine transporter (NET) is responsible for removing NE from the synaptic cleft and extracellular milieu following neurotransmitter release. NET is the target of multiple pharmacotherapies including desipramine, duloxetine and milnacipran, highlighting its regulatory function (or dysregulation) in numerous disorders. Besides its native substrate, NET has been shown to bind and transport synthetic analogues of neurotransmitters and neurotoxins.[62,63,64] For instance the binding and transport of a cationic probe, **ASP**$^+$, was reported by DeFelice,[63] and described here is a related stilbazolium dye, **HNEP**$^+$, that is also transported by NET.[64] We recently investigated binding and transport limits of NET using a series of bifunctional cationic fluorophores embedded with stilbazolium dimers connected by a flexible six-carbon as probes.[65]

3.2. Structure of Stilbazolium Dyes

The electronic structures of stilbazolium dyes consist of donor and acceptor moieties linked by π-bonds. They can simply be considered as donor-π-acceptor systems. One of the well-studied stilbazolium dyes is Brooker's merocyanine (1-methyl-4-[(oxocyclohexadienylidene)-ethylidene]-1,4-dihydropyridine),[66] **BM** (Figure 3.0) exhibits remarkable solvatochromism and serves as a model for other solvatochromic dyes and environmentally sensitive fluorophores.[58,59,29,67] In this chapter, we focus on the photophysics of a relatively rigid 4-[2-(6-hydroxy-2-naphthalenyl)-ethenyl]-1-methyl-pyridinium (**HNEP**$^+$), a benzo-fused analogue of **BMH**$^+$, that functions as a ligand and transporton[68] of the norepinephrine transporter (NET).[64, 65]

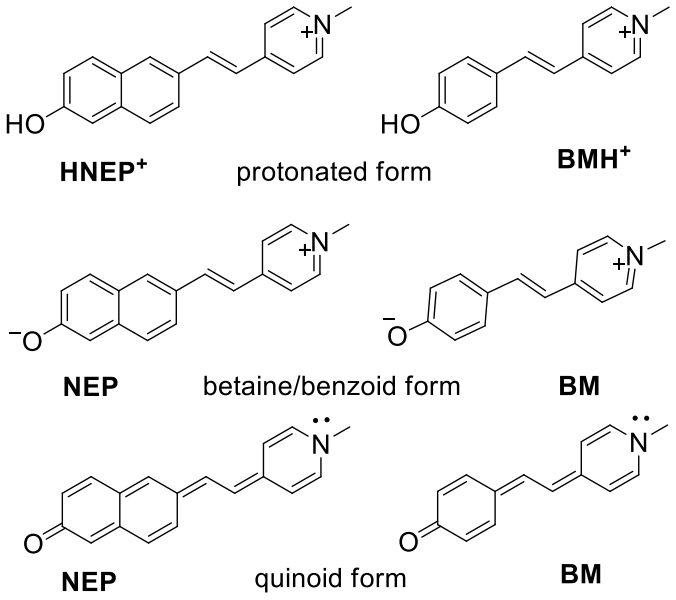

Figure 3.0 Structures of **HNEP**$^+$/**NEP** and Brooker's merocyanine, **BMH**$^+$/**BM**.

BMH$^+$ and **HNEP**$^+$ exhibit different optical or electronic properties in spite of their homologous structures.[69] One marked difference is the effect of solvent on the photoemission of these two molecules. In water the emission of both **BMH**$^+$ and **HNEP**$^+$ is quenched ($\Phi_{em} \approx 0.01$), however, in octanol the emission of **BMH**$^+$ only doubles (Φ_{em}

= 0.02) while that of **HNEP**$^+$ is enhanced approximately 16-fold (Φ_{em} = 0.16). This emission enhancement enables **HNEP**$^+$ to function as a "turn-on" fluorescent probe when bound to NET and other cellular targets such as mitochondria. It is not immediately clear why benzo-fusion in **HNEP**$^+$ should contribute to a higher degree of emission enhancement compared to **BMH**$^+$. A possible explanation is that **HNEP**$^+$ does not exhibit a similar degree of charge transfer character; the increase in length could lead to decreased electronic coupling between the electron-withdrawing pyridinium moiety and electron-donating naphthol. The increase in length on one hand may lead to enhanced solvent sensitivity due to a larger change in dipole between the ground and excited states. Protonation state may also play a role in controlling fluorescence, with the deprotonated form, **NEP**, potentially existing in two canonical forms; a zwitterionic betaine or neutral quinoid, that have been described for **BM**.[29,67]

We investigated the photophysics of **HNEP**$^+$/**NEP** with focus on two key solvent parameters, pH and polarity using UV-vis and fluorescence spectroscopy. Quantum chemical calculations were also utilized to gain insights into the relevant participating molecular orbitals.

3.3. Optical Spectroscopy

UV-vis and emission spectroscopy were carried out in phosphate buffered solutions with pH range of 2.0 to 12.0. This is first to establish the pKa of **HNEP**$^+$ in the ground and the excited states in order to distinguish between the protonated and neutral forms. Second, to examine the solvatochromic behavior of **HNEP**$^+$ and **NEP** in order to evaluate the relative polarities of the ground and the excited states.

3.4. Determination of pKa from Absorption and Emission Spectroscopy

In neutral and acidic solutions, the absorption maximum of **HNEP**$^+$ was found to be 390 nm (Figure 3.1A), and beyond pH 7.5 a new absorption band at 455 nm was produced with a simultaneous decrease in the peak at 390 nm. A visible isosbestic point at 412 nm in the overlaid spectra specify a transition between two species; the protonated, cationic form, **HNEP**$^+$ at low pH and the neutral form, **NEP** at higher pH values. A pKa of 9.0 (Figure 3.1B), comparable to the value reported for **BMH**$^+$/**BM** (pKa = 8.6)[57] was obtained from the plot of the ratio of the absorbance values ($A_{455\ nm}/A_{390\ nm}$) with pH.

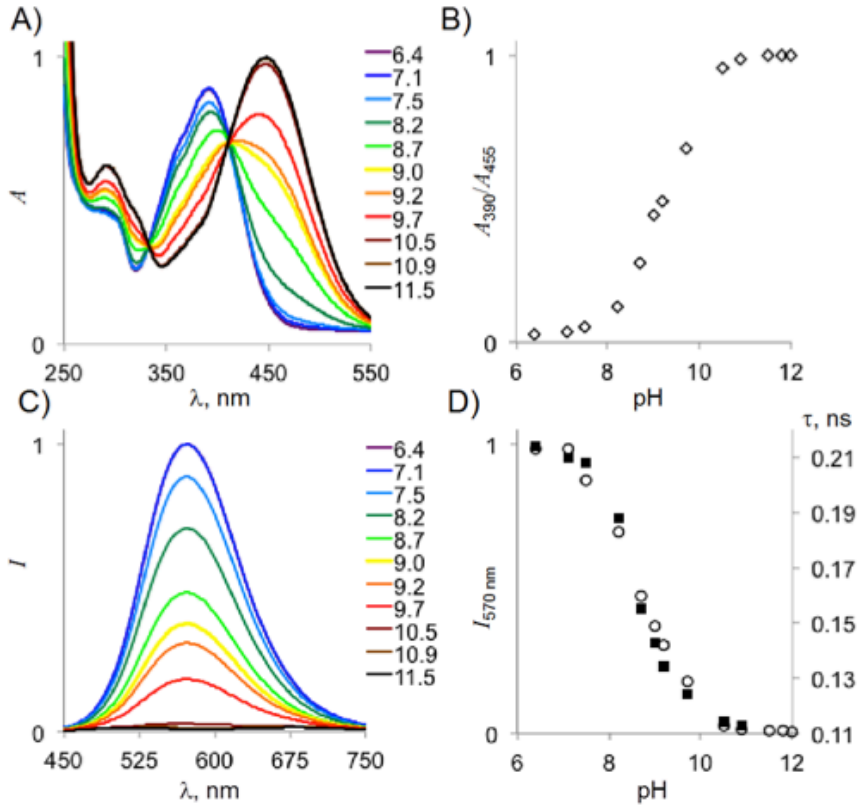

Figure 3.1 Spectroscopic determination of pKa of **HNEP**$^+$/**NEP**. (A) At neutral and acidic pH values, a single peak at 390 nm is visible; increasing the pH beyond 7.5 leads to the appearance of a peak at 455 nm due to the presence of **NEP**. (B) Plot of the ratio of A_{455}/A_{390} vs pH. (C) pH dependent emission of **HNEP**$^+$/**NEP**: with increasing pH and lowering concentration of **HNEP**$^+$, the emission centered at 570 nm decreases. (D) Plot of the intensity at 570 nm vs pH superimposed on the emission lifetime values.

The existence of transition between the two species within the same pH range was confirmed by the emission spectra. **HNEP**$^+$ is weakly fluorescent ($\Phi_{em} \leq 0.01$) in acidic and slightly basic solutions, but exhibits a clear emission peak centered at 565 nm (Figure 3.1C). For solutions with pH above 8, the emission intensity decrease and is below detection ($\Phi_{em} << 10^{-3}$) above pH 10.9. The emission lifetime and intensity show good correlation over the same pH range (Figure 3.1D). A maximum lifetime of 0.22 ns is found at low pH, which decreases to 0.11 ns at pH 10.9, and cannot be measured beyond pH values above 10.9 due to low Φ_{em}. The data from both steady state emission and emission lifetime indicate a pKa of 8.8 for **HNEP**$^+$, which correlates well with the value revealed from UV-vis spectroscopy.

3.5. Solvatochromism

Merocyanine dyes may display positive or negative solvatchromism depending on the polarity of the excited state relative to the ground state.[70] Positive solvatochromism implies an excited state of higher polarity, while negative solvatochromism indicates a more polar ground state. This behavior can be quite large for zwitterionic dyes. For example, **BM** shows a difference of 143 nm in the lowest energy absorption band between acetone (λ_{max}, abs = 585 nm) and water (λ_{max}, abs = 442 nm).[71]

Absorbance of **HNEP**$^+$ and **NEP** were measured in twelve protic and aprotic solvents with polarities ranging from 63.1 kcal/mol (H_2O) to 37.4 kcal/mol (THF) based on Reichardt's ET (30) scale (Figure 3.2).[46] The plots for **BMH**$^+$ and **BM** are also shown for comparison.[71]

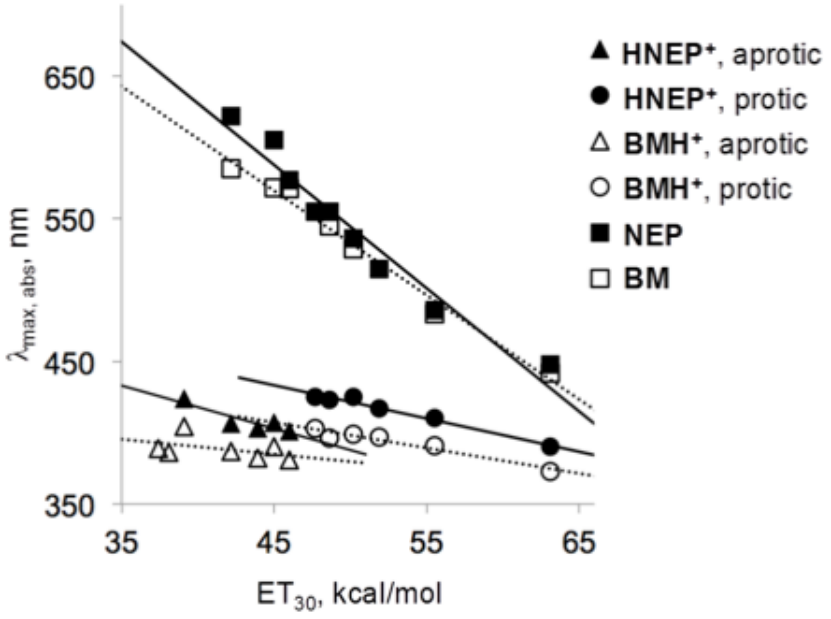

Figure 3.2 Plot of $\lambda_{max,\ abs}$ versus solvent polarity (using Reichardt's ET_{30} scale). **HNEP**$^+$ and **NEP** exhibit a negative solvatochromic effect that is larger than **BMH**$^+$ and **BM** in both protic and aprotic solvents. The separate fits for protic and aprotic solvents for **HNEP**$^+$ suggests a hydrogen-bonding in protic solvents similar to that previously observed for **BMH**$^+$.

HNEP$^+$ and **NEP** display negative solvatochromism in both aprotic and protic solvents. **HNEP**$^+$ shows absorption maxima of 390 nm in H_2O and 425 nm in octanol and $CHCl_3$. Linear regression analysis for **HNEP**$^+$ in protic and aprotic solvents produce apparent $R^2 = 0.97$ and 0.79 respectively. This may possibly be due to hydrogen bonding interactions, which has previously been observed for **BMH**$^+$/**BM**.[71] **NEP** exhibits larger solvatochromic effect with absorption maxima ranging from 448 nm in H_2O to 622 nm in acetone. The negative solvatochromic effect of both **HNEP**$^+$ and **NEP** is somewhat larger than that for **BMH**$^+$ and **BM**. This may be due to a larger change in the dipole moments for **HNEP**$^+$/**NEP** between the ground and the excited states, which can be rationalized if

a similar redistribution of charges occur over the longer benzofused derivative upon photoexcitation.

Figure 3.3 shows the colors observed in six selected solvents with their corresponding absorption spectra; the colors range from orange (MeOH) to deep purple (AcCN). The deeply colored solutions that can be easily distinguished by eye may arise from the relatively long wavelength absorption bands of **NEP**.

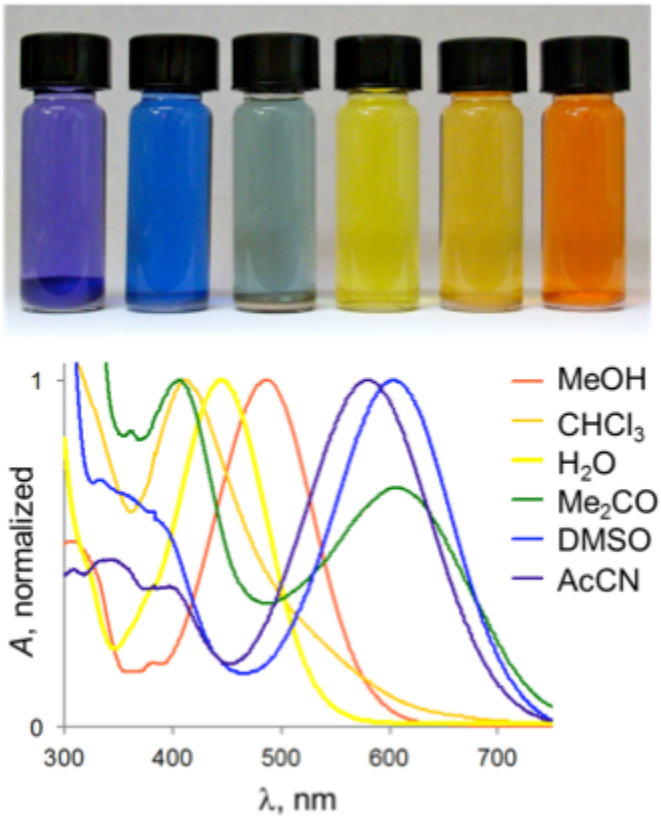

Figure 3.3 Solvatochromicity of **NEP**: at top, photograph of **NEP** solutions (left to right: AcCN, DMSO, Me_2CO, H_2O, $CHCl_3$, MeOH); at bottom, normalized absorption spectra of 10 μM solutions.

For **NEP**, no disconnect between protic and aprotic solvents is apparent from linear regression analysis (R^2 = 0.95). In the less polar solvents, such as $CHCl_3$ (Figure 3.3), **NEP** corresponds to the clear long wavelength absorption band with only a broad tail

extending into lower energies. A possible explanation for this observation is that **NEP** preserves strong betaine character rather than existing in the quinoidal form; as less polar solvents do not readily accommodate the dipolar species, this shifts the equilibrium to the protonated form. This view is partly confirmed by the ease with which **BMH**$^+$ converts to the neutral form, **BM**, in less polar solvents such as EtOAc and THF (Figure 3.4); in the same solvents, only a small fraction of **NEP** is evident.

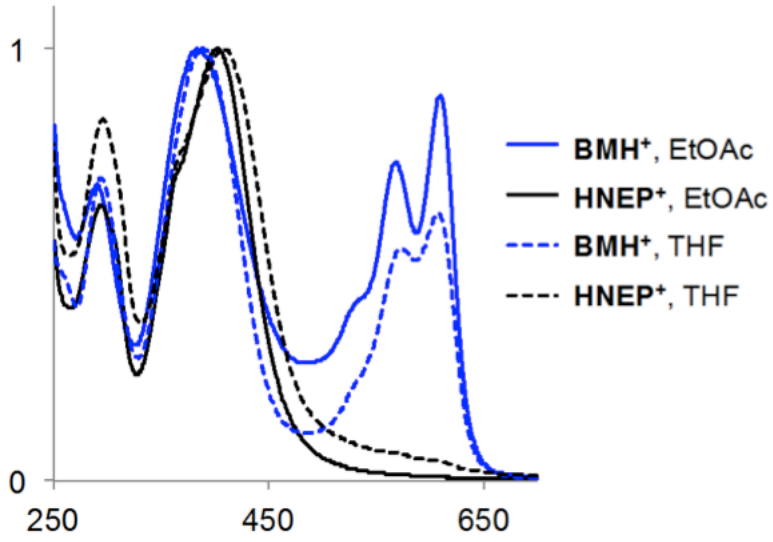

Figure 3.4 Comparison of the UV-vis spectra of **HNEP**$^+$ and **BMH**$^+$ in solvents of low polarity. **HNEP**$^+$ remains protonated while **BMH**$^+$ is readily deprotonated without the addition of base and achieves the neutral quinoidal structure as evidenced by the well-defined peaks above 500 nm.

The line shape of the lowest energy absorption band of **BM** and **NEP** also provides some insight into the nature of these electronic transitions. **BM** possesses vibronic structure (Figure 3.4, in blue), while **NEP** exhibits a typical charge transfer process marked by broad and structureless absorption band. This behavior can be explained in part by the relative instability of 2,6-naphthoquinones, which are regarded as nonaromatic.[72, 73]

Table 3.1 Solvent dependent **HNEP**$^+$/**NEP** absorption and emission parameters.

Solvent	$\lambda_{max,\ abs}$ (nm)[a]	$\lambda_{max,\ em}$ (nm)[a]	$\Delta\nu$ (cm^{-1})[a]	Φ_{em}[a]	$\lambda_{max,abs}$ (nm)[b]
H_2O	390	565	7940	0.01	448
MeOH	409	571	6880	0.08	486
EtOH	416	567	6340	0.09	515
2-propanol	426	563	5770	0.12	536
1-butanol	424	563	5820	0.09	555
1-octanol	426	556	5540	0.16	555
AcCN	400	557	7050	0.23	577
DMSO	408	565	6800	0.06	605
Ac_2O	403	561	6800	0.34	-
Me_2CO	406	561	6990	0.19	622
$CHCl_3$	424	537	4960	0.03	-
THF	412	560	6410	0.19	-

[a]**HNEP**$^+$, [b]**NEP**

While **HNEP**$^+$ is weakly to moderately emissive in the solvents investigated (Table 3.1), no emission for **NEP** could be detected. The difference in ground state and excited state dipoles can be calculated from a Lippert plot:[74] the slope obtained from a plot of the Stokes shift ($\Delta\nu$) versus the solvent orientation polarizability yields the term $2(\Delta\mu)^2/hcr^3$ (Figure 3.5). The value of Onsager cavity radius r, can be estimated as half the maximum charge displacement of the dye. Thus, $\Delta\mu$ for the $S_0 \rightarrow S_1$ transition for **HNEP**$^+$ is calculated as 17.9 D in protic solvents and 16.4 D in aprotic solvents. While these values are only approximate, they nonetheless agree very well with the change in dipole moments predicted from quantum chemical calculations detailed below. Furthermore, these values compare very well with those calculated for **BMH**$^+$ (12.8 D for protic solvents and 10.7 D for aprotic solvents). Certainly, the difference in dipoles between these two species is a direct consequence of difference in their lengths due to benzofusion.

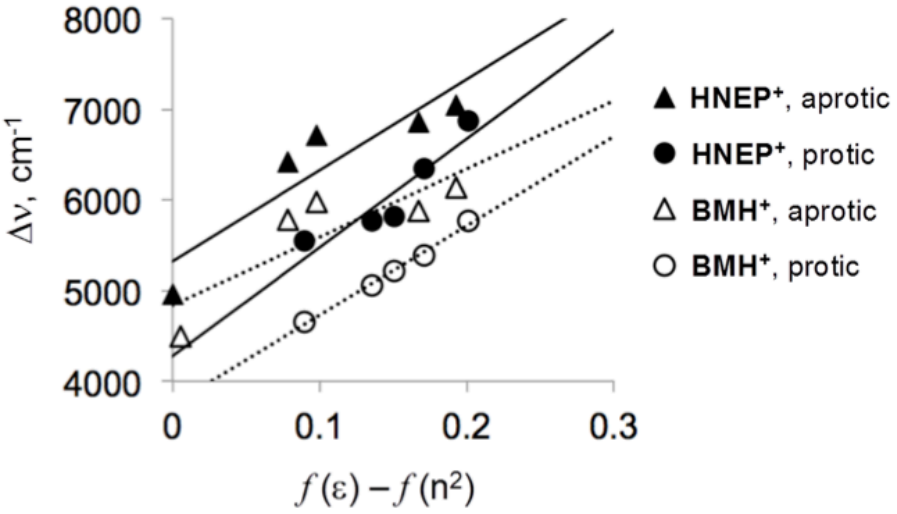

Figure 3.5 Plot of the Stokes shift (Δν) of **HNEP**$^+$ (Table 3.1) and **BMH**$^+$ vs the solvent polarity function $f(\varepsilon) - f(n^2)$. The slope of the line corresponds to the term $2(\Delta\mu)^2/hcr^3$.[73,74] For **HNEP**$^+$, $\Delta\mu$ = 17.9 D (R^2 = 0.87) and 16.7 D (R^2 = 0.83) in protic and aprotic solvents respectively.

3.6. Quantum Calculations

The molecular orbital contributions to the observed optical transitions and solvatochromicity were investigated with a time-dependent density functional theory (TD-DFT) calculations on **HNEP**$^+$ and **NEP** using the B3LYP and CAM-B3LYP methods[75] at the 6-31G(d) level and Truhlar's universal solvation model (SMD)[76] in Gaussian 09.[54] Murugan et al. highlighted the importance of including explicit solvent molecules when dealing with hydrogen bonding media in their study of **BM** and other authors have noted the challenges in accurately accounting for solvation of the neutral and zwitterionic states.[70] In the present case, the inclusion of a protic solvent molecule (H_2O, MeOH or EtOH), that hydrogen bonds with the naphthol oxygen, gives results consistent with the experimentally determined values for the transition energies (Figure 3.6).

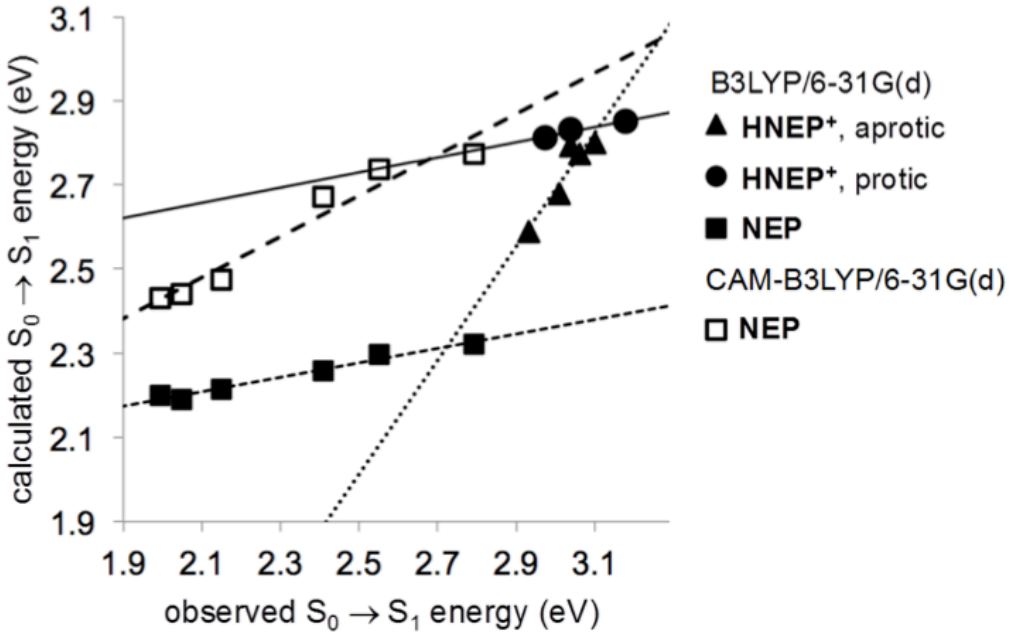

Figure 3.6 Plot of calculated versus observed $S_0 \rightarrow S_1$ transition energies for **HNEP**$^+$ and **NEP** in different solvents. Although the transition energies are correctly ordered, the solvatochromic effect is overestimated (**HNEP**$^+$, aprotic) or underestimated (**HNEP**$^+$, protic; **NEP**, all solvents).

Using the B3LYP density functional, the solvatochromic effect is overestimated for **HNEP**$^+$ in aprotic solvents and underestimated in protic solvents; the effect was also underestimated for **NEP** in all solvents examined. The CAM-B3LYP functional more accurately accounts for the CT absorption of **NEP**, but was unable to accurately account for the $S_0 \rightarrow S_2$ transitions of **HNEP**$^+$ and was not included in our analysis. In all cases (**HNEP**$^+$/aprotic solvents, **HNEP**$^+$/protic solvents, **NEP**/all solvents), the transition energies are correctly ordered according to the negative solvatochromicity and therefore the methods are expected to accurately predict most aspects of the electronic transitions.

The TD-DFT calculations reveal the origin of several additional spectroscopic features of **HNEP**$^+$ and **NEP**. For **HNEP**$^+$ the $S_0 \rightarrow S_2$ transition is predicted at slightly higher

energies and lower oscillator strength than the $S_0 \rightarrow S_1$ transition; it is evident as a modest shoulder at approximately 360 nm in Figure 3.1A, which is in good agreement with the predicted value of 347 nm. The modest spatial overlap of the $HOMO^{-1}$ and LUMO (Figure 3.7) contributes to the lower probability of this transition. For **NEP** no such shoulder is visible which is consistent with the calculations of negligible oscillator strength for the $S_0 \rightarrow S_2$ and $S_0 \rightarrow S_3$ transitions resulting from the poor overlap of HOMO with $LUMO^{+1}$ and $HOMO^{-1}$ with LUMO, respectively.

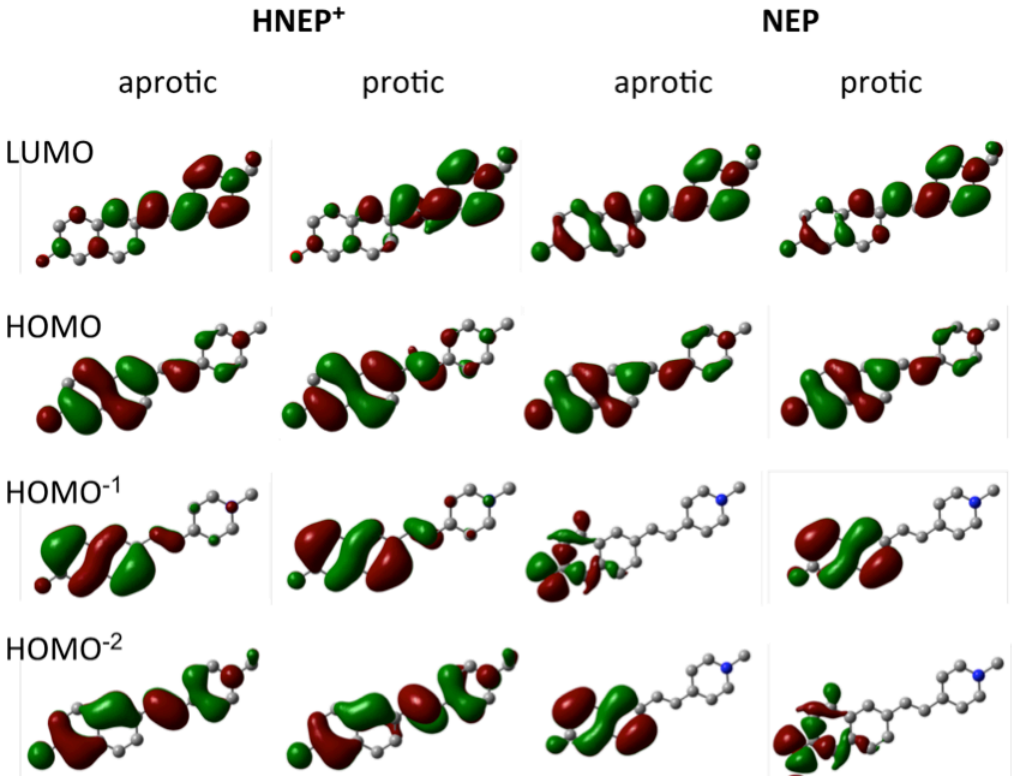

Figure 3.7 Calculated frontier molecular orbitals plus $HOMO^{-1}$ and $HOMO^{-2}$ for **HNEP**$^+$ and **NEP** in representative aprotic (Me_2CO) and protic (H_2O) solvents

Inspection of the frontier molecular orbitals of **HNEP**$^+$ and **NEP** reveals that the lowest energy transition is $\pi \rightarrow \pi^*$ in nature with significant charge transfer character owing to the polarized frontier molecular orbitals.[77] The HOMO is polarized towards the

electron donating naphthol/naptholate while the LUMO is polarized towards the electron-withdrawing pyridinium moiety. The redistribution of charge should result in an excited state with a smaller dipole than the ground state, i.e. $\mu_{ES} < \mu_{GS}$. For **HNEP**$^+$, the difference in dipoles ($\mu_{GS} - \mu_{ES}$) is calculated to be 10.9 D in THF and 10.8 D in H_2O, which compares favorably to the experimentally determined values of 16.7 D in aprotic solvents and 17.9 D in protic solvents given the assumptions regarding charge displacment.[78] For **NEP**, $\mu_{GS} - \mu_{ES}$ could not be determined from the spectroscopic data as no emission was observed. However, based on the observed negative solvatochromicity, it is expected that the ground state possesses a large dipole that is more strongly stabilized in protic solvents; DFT calculations account for this effect with μ_{GS} = 48.7 D in H_2O and μ_{GS} = 39.9 D in acetone. The negative solvatochromism of **NEP** indicates that the excited state should be less polar; this is also accurately predicted by TD-DFT, with μ_{ES} = 23.1 in H_2O and μ_{ES} = 18.3 D in acetone. The calculated change in dipole between the ground and the excited states is larger for H_2O ($\mu_{GS} - \mu_{ES}$ = 25.6 D) compared to acetone ($\mu_{GS} - \mu_{ES}$ = 21.6 D), in good agreement with the experimentally observed solvatochromicity.

The molecular orbital diagram (Figure 3.7) shows that the Kekulé representation of **NEP** (Figure 3.0) as either the neutral quinoidal form or zwitterionic benzoid form oversimplifies the true electronic structure and corresponding optical transitions. Regardless of protonation state or solvent, the HOMO has consistent contribution of a p orbital from the naphthol/naphtholate oxygen. The representation of **NEP** as a zwitterion or neutral compound does not entirely capture this fact and can somewhat skew the notion of charge stabilization and related optical transitions. Deprotonation of **HNEP**$^+$

does elevate a low-lying ($HOMO^{-7}$), σ-type MO to a high energy, non-bonding MO of **NEP** (Figure 3.7). The zwitterionic character of **NEP** can be directly linked to this high lying nonbonding orbital, which is stabilized in protic solvents ($HOMO^{-2}$) relative to aprotic solvents ($HOMO^{-1}$). However, it is not expected that this orbital contributes to any of the observed solvatochromicity as the transition would be weak owing to the n→π* character, indeed, the calculated oscillator strength is less than 0.05 in both protic and aprotic solvents. Therefore, the observed solvatochromicity of **NEP** appears to be the result of polarization of HOMO and LUMO; in protic solvents, less HOMO density is observed on the pyridinium ring, while the LUMO has less density on the naphthalene moiety.

3.7. Conclusions

We have investigated the photophysical behavior of a benzofused analogue of Brooker's merocyanine in relation to protonation state as well as solvent polarity. From UV-vis and fluorescence studies, we find that **$HNEP^+$/NEP** share several common features with **BMH^+/BM**. First, **$HNEP^+$** and **BMH^+** possess a similar pKa value, which accords their similar molecular architecture. Second, both dyes exhibit negative solvatochromicity, which is more pronounced for their neutral forms, **NEP** and **BM**. The moderately larger solvatochromism observed for **NEP** indicates that there are some differences in the electronic structures compared to **BM**. One notable aspect is that **NEP** exhibits a greater degree of charge transfer upon photoexcitation as revealed by the unstructured absorption peaks. Quantum chemical calculations provide insights into the optical transitions and contributing molecular orbitals demonstrating that although **NEP** does exhibit zwitterionic character, this is mostly the result of a non-bonding MO that

does not contribute to the observed optical transitions. Instead, frontier orbital polarization appears to be the underlying phenomenon responsible for the high solvatochromicity.

3.8. Experimental Methods

3.9. Steady-State Emission and Absorption Spectroscopy

Spectroscopy and HPLC grade solvents were utilized for all spectroscopic measurements; all path lengths were 1 cm. UV-vis absorption spectra were obtained on a Perkin-Elmer Lambda 35 UV-vis spectrometer using chromophore solutions of 10 μM. Fluorescence studies were performed on a Perkin-Elmer LS55 Fluorometer. Trace water alters the $\lambda_{max,\ abs}$ of **NEP**, therefore UV-vis and emission solutions were prepared immediately before spectroscopic measurements (from 10 mM DMSO stocks; final concentration of DMSO was 0.1% in the actual solvent used) and kept dry with solid K_2CO_3. Deprotonation of samples were carried with triethylamine (purity ≥ 99.5%). For determination of Φ_{em}, solutions were prepared to an optical density of less than 0.05 in order to minimize inner filter effects. Perylene in cyclohexane was used as a reference for quantum yields.[51] Fluorescence lifetimes were obtained on a frequency-domain lifetime spectrometer ChronoFD from ISS exciting at 370 nm using POPOP or 1,4-bis(5-phenyloxazol-2-yl)benzene (scintillation grade) in ethanol as a standard.

3.10. Computational Methods

Quantum chemical calculations were carried out utilizing the Gaussian ’09 suite of electronic structure modeling software.[54] Ground state geometries of the dyes with and without explicit solvent molecules were optimized by DFT with the B3LYP/6-31G(d) method using Truhlar’s SMD solvation model. Vertical transition energies were obtained

by TD-DFT calculations with the B3LYP/6-31G(d) method and CAM-B3LYP/6-31G(d) method[75] with the SMD model. Molecular orbitals were visualized using the GaussView 5 program.

CHAPTER 4

Assessing Single-Step Charge Transfer Complexes using π−π Interactions

4.1 Overview and Significance of Polycyclic Aromatic Molecules

Polycyclic aromatic molecules (PAMs) with well-defined optical and electronic properties serve as photoactive materials in organic electronics, fluorescence based sensing, and in supramolecular chemistry.[79,80] In most applications, the optoelectronic properties of these materials are dependent not only on their chemical composition, but also on intermolecular interactions, orientation and long-range order. Tight control of molecular morphology often necessitates chemical modification of the photoactive materials to introduce recognition elements that help define supramolecular structure.[80,81,82] In some cases, however, aromatic interactions alone can drive molecular assembly and dictate the resulting electronic processes.[5,81] The self-organization of π-electron donor and acceptor blend can give rise to enhance performance of organic photovoltaics through selective, segregated stacking of the individual components.[83,84,8] On the other hand, mixed columnar stacks of π electron donors and acceptors can yield binary materials with tunable charge transfer (CT) energies and enhanced allowability.[85,86] These alternate morphologies for donor-acceptor blends point to the difficulty in predicting CT interactions and describing π-π interactions in general.

Indeed, several theoretical descriptions have been developed, which emphasize to varying degrees, the importance of geometry and orientation of the aromatic structure, the size, shape and symmetry of the frontier molecular orbitals (FMO) and the energy gap in complex array of donors and acceptors.[5,17,87] Our recent investigations of CT complexes

have shown that orbital congruency plays an important role in the strength of these aromatic interactions, which can yield selective π- stacking pairs and luminescent solid-state complexes.[88,89] Interestingly, the role of orbital interactions in the preferential formation of CT-complexes is entirely consistent with the Salem-Klopman[90] treatment of molecular complexes:

$$\Delta E = \underbrace{-\sum_{ab}(q_a + q_b)\beta_{ab}S_{ab}}_{first\ term} + \underbrace{\sum_{k<l}\frac{Q_k Q_l}{\varepsilon R_{kl}}}_{second\ term} + \underbrace{\sum_{r}^{occ.}\sum_{s}^{unocc.} - \sum_{r}^{occ.}\sum_{s}^{unocc.}\frac{2(\Sigma_{ab}C_{ra}C_{sb}\beta_{ab})^2}{E_r - Es}}_{third\ term} \qquad 1$$

The third term highlights the importance of orbital interactions (*a* and *b* represent atomic orbitals, c_{ra} is the coefficient of atomic orbital *a* in molecular orbital *r*, c_{sb} is the coefficient of atomic orbital *b* in molecular orbital *s*, and β is resonance integral) as well as the difference in energies between the interacting molecular orbitals (E_r-E_s). For CT complexes, the orbitals of primary concern should be the HOMO of the electron donor and the LUMO of the electron acceptor. This difference in energies between these two orbitals can also be linked to the second term of the Salem-Klopman equation, as in many cases, the chemical modifications that manipulate the energy of the HOMO and LUMO also serve to increase and decrease the electron density of the π-system. The notion of orbital symmetry in π-π stacking is not at odds with other descriptions of aromatic interactions, such as Hunter's model,[5,18] and has also been noted in other systems as well. Kato et al. rationalized the preferential binding of a pyromellitic diimide (PMI) cyclophane with α-naphthol over β-naphthol on the basis of orbital interactions.[91] A third factor influencing the binding energy is the size of the interacting aromatic molecules, which correlates with stabilization energy arising from dispersion interactions.

Additionally, increasing the number of participating p orbitals also serves to decrease the HOMO-LUMO gap, which increases the stabilization energy seen in the third term of equation 1.

The operation of any optically controlled device depends on the efficient absorption of light by the chromophore and its ability to undergo electron transfer. Although direct excitation of electrons from the HOMO of the donor to the LUMO of the acceptor in a single-step could be much faster in molecules with high molar absorptivity, their narrow absorption band width, in some cases, necessitate incorporation of light-absorbing antenna molecules to enhance their spectral coverage.[92] The molecules should exhibit suitable redox potential to generate free charges on absorption of photons. Thus, by selecting molecules based on their spectral and electrochemical properties, it should be possible to cover any region of the visible spectrum.[92] However, most of the well-studied molecular systems generally have low molar absorptivity (less than 200 M^{-1} cm^{-1}).[4,9,13,20,93] Our group[89] recently reported molar absorptivity greater than 500 M^{-1} cm^{-1} in solution and 5000 M^{-1} cm^{-1} in solid state for naphthalene diimide (**NDI**) with pyrene and its derivatives, a condition crucial for direct excitation of electron from the donor's HOMO to the LUMO of the acceptor. The relative contributions of geometric size, HOMO-LUMO energy gap and FMO features toward π-stacking interactions can be difficult to compare in dissimilar molecular constructs. A rational approach is to correlate these factors with the magnitude of experimentally determine charge-transfer constants. Such correlation could serves as a basic tool for selecting potential donor-acceptor pairs, where electrons could be excited directly from the donor to the acceptor.

In this section, we investigate the strength of CT form across a series of PAMs to explore the relative effects of size, orbital topology and energy using spectroscopic (^{1}H NMR, UV-visible and steady state fluorescence) techniques. Seven π-electron donors and two π-electron acceptors (Figure 4.0), which exhibit desirable characteristics including high molar absorptivity,[89] redox potential (Table 4.1) and FMO (Figure 4.1) were selected for this spectroscopic study. The results clearly show that high molar absorptivity enhanced high CT formation, while energy difference between the HOMO-LUMO, π-surface area, symmetry, shape and size of frontier molecular orbital dictate the molecular orientations or ordering and hence the strength of CT complex formation.

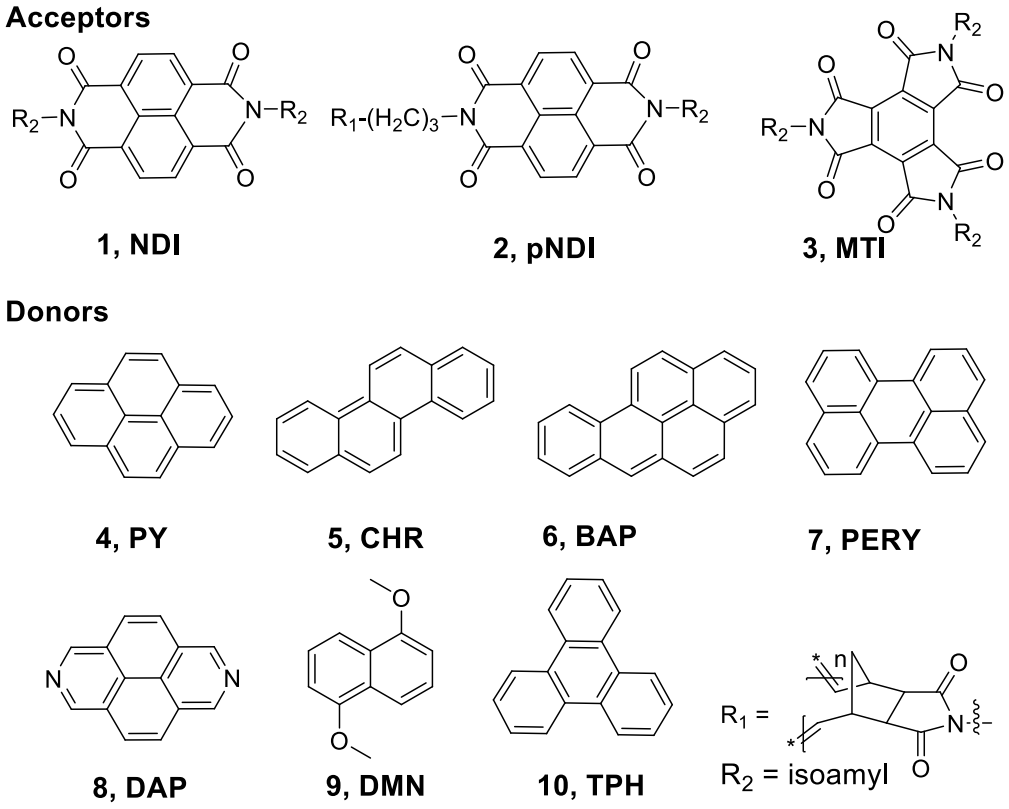

Figure 4.0 Chemical structures of acceptors (**1**-**3**) and donors (**4**-**10**) studied. Abbreviations **NDI** = naphthalene diimide, **MTI** = mellitic triimide, **PY** = pyrene, **CHR** = chrysene, **BAP** = benzo[a]pyrene, **PERY** = perylene, **DAP** = 2,7-diazapyrene, **DMN** = 1,5-dimethoxynaphthalene, **TPH** = triphenylene.

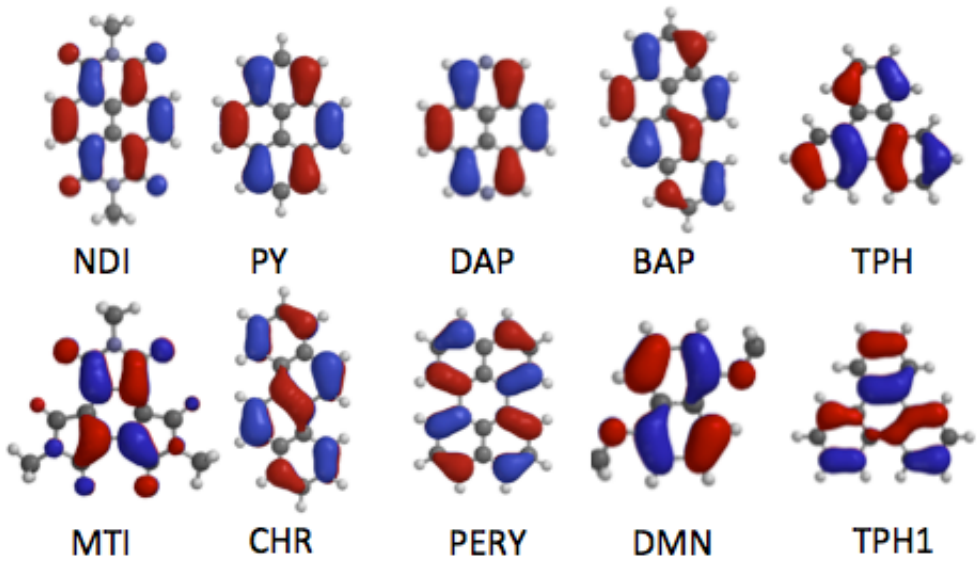

Figure 4.1 Optimized geometries of acceptors' LUMOs and donors' HOMOs calculated in the gas phase. **NDI** exhibits high orbital congruency with **PY** and **DAP** respectively, which is slightly distorted in case of **BAP**. Orbital of **MTI** matches well with that of **DMN** and **TPH**.

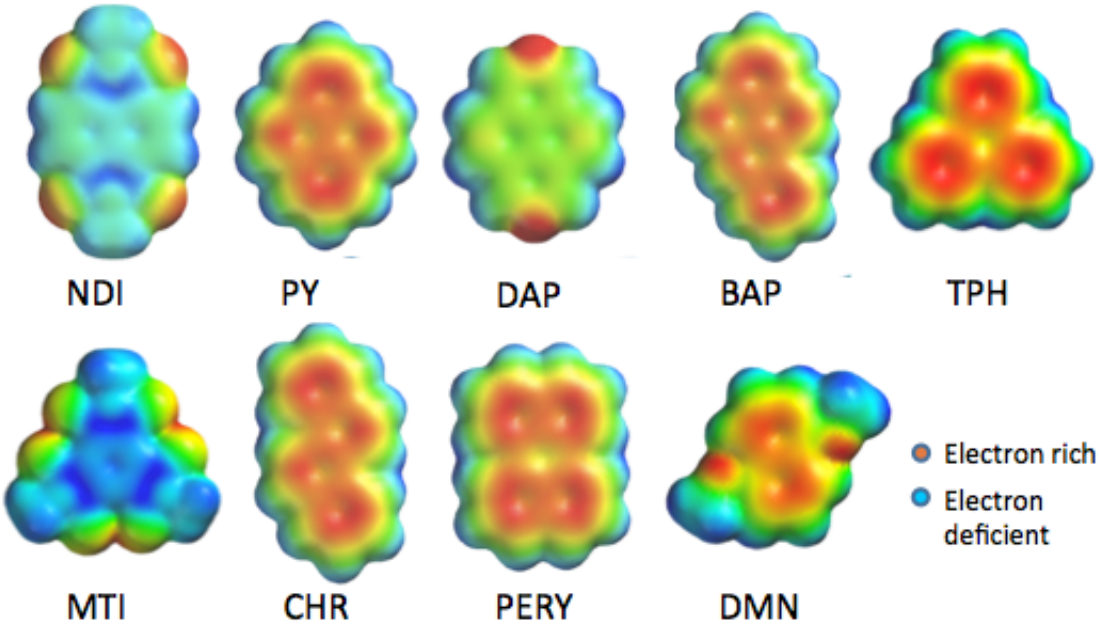

Figure 4.2 Electrostatic potential maps for acceptors and donors. **NDI** and **PY** display harmonious surfaces, while **DAP** surface is deficient of electrons despite its comparablegeometry with **NDI** and **PY**. **MTI** surface matches well with that of **TPH**. **PERY** shows a centro-symmetric surface.

Table 4.1 Redox potentials,[1] energy and area of donors and acceptors.

Molecule	E_{ox}(V)	E_{red}(V)	E_{HOMO}(kJ/mol)	E_{LUMO}(kJ/mol)	Area(Å)
DAP		-2.54[a]	-587.36		209.54
CHR	1.59,[b] 1.40[c]	-2.01[b]	-556.28		250.46
PY	1.40,[b] 1.36[d]	-1.85,[b] -2.04[d]	-537.11		219.91
PERY	1.09,[b] 1.06[d]	-1.43,[b] -1.66[d]	-500.81		261.83
TPH	1.79,[b]	-2.22[b]	-590.01		243.12
DMN	1.52,[b] 1.28[e]	-2.52,[b] -2.75[e]	-124.29		218.47
BAP	1.18,[b] 1.16[d]	-1.86,[b] -1.84[d]	-515.53		264.22
NDI		-0.45,[f] 0.651,[g*] -1.0[g**]		-316.73	274.06
MTI		-0.58,[h*] -1.25[h**]		-73.41	304.02
*First reduction potential		**Second reduction potential			

4.2 Spectroscopic Techniques

The CT constants for various complex systems were determined with ^{1}H NMR due to the insensitivity of chemical shift of molecule of interest to small concentration of impurities, the use of line position instead of intensities and degree of independence in cases where more than one probe in a molecule are considered.[94] In complexes where association constants could not be determined as a results of experimental constraints including invisibility of chemical shifts of interest, UV-visible and steady state fluorescence techniques were employed to quantify the magnitude of the π–π interactions.

---

[a] Waldhör, E.; Zulu, M.M;Zalis, S.;Kaim, W.,*J. Chem. Soc. Perkin Trans. 2* **1996**, 1197
[b] Crespo-Hernández, C.E.; Close, D.M.; Gorb, L.; Leszczynski, J.,*J.Phys. Chem. B* **2007**, *111*, 5386-5395
[c] Allison, D.; Kim, M.-H.,*Microchem. J.* **1993**, *47*, 172-177
[d] Wilson, J.N.; Cho, Y.; Tan, S.; Cuppoletti, A.; Kool, E.T.,*ChemBioChem,* **2008**, *9*, 279-285
[e] Zweig, A.; Maurer, A.H.; Roberts, B.G.,*J. Org. Chem.* **1967**, *32*, 1322-1329
[f] Kumar, N.S.S.; Gujrati, M.D.; Wilson, J.N.,*Chem. Commun* **2010**, *46*, 5464-5466
[g] Erten, S.; Alp, S.; Icli, S., *J. Photochem. Photobio. A* **2005**, *175*, 214-220
[h] Carroll, J.B.; Gray, M.; McMenimen, K.A.; Hamilton, D.G.; Rotello, V.M.,*Org. Lett.* **2003**, *5*, 3177-3180

4.3 ^{1}H NMR Studies: Association constant (K_A), Entropy and Enthalpy

The aromatic protons of monomer **1** were found to exhibit an upfield shift with respect to both concentration and temperature (figure 4.3), an indication of π-stacking interactions.

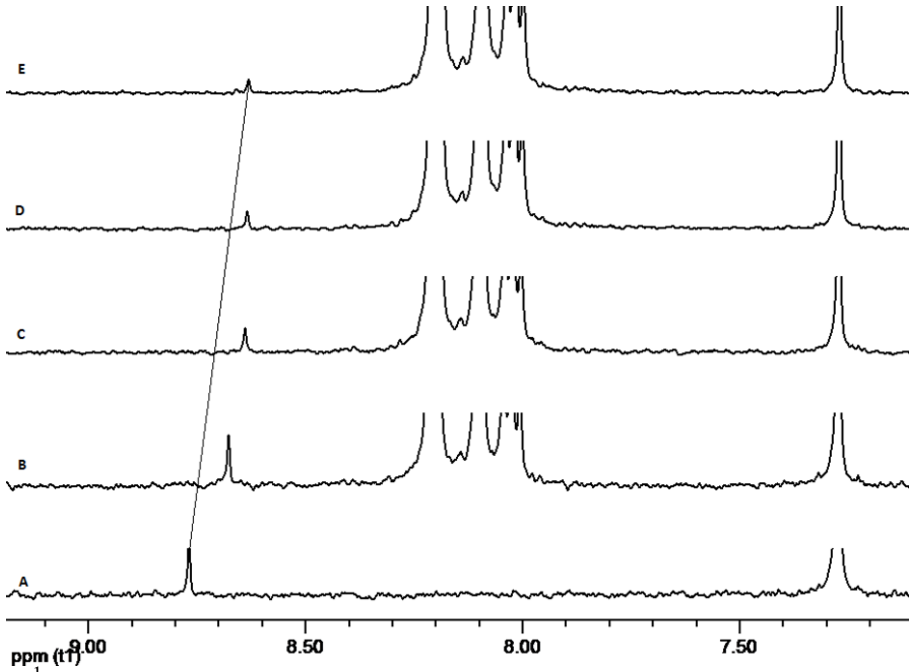

Figure 4.3 ^{1}H NMR titration of **NDI** with PY; 500μM **NDI** in (a) alone @ 24°C (b) 9.3 mM **PY** @ 24°C (c) 15.8 mM **PY** @ 32°C (d) 20.8 mM **PY** @ 40°C (e) 24.7 mM **PY** @ 47°C. Aromatic protons of **NDI** are shifted downfield with respect to temperature and upfield shift with concetration; upfield shift for both temperature and concentration.

Table 4.2 Thermodynamic parameters of donor-acceptor CT complexes from ^{1}H NMR titration at 298 K.

Entry	Donor	Acceptor	$K_A(M^{-1})^a$	ΔG(kcal/mol)	ΔH(kJ/mol)	ΔS(J/mol·K)
1	**NDI**	**NDI**	44.0	-2.22	26.16	115.59
2	**PY**	**NDI**	9.6	-1.36	-11.97	-21.20
3	**CHR**	**NDI**	6.1	-1.04	-11.89	-25.48
4	**PERY**	**NDI**	79.6	-2.61	-20.40	-31.87
5	**BAP**	**NDI**	9.7	-1.34	-26.75	-70.41
6	**DAP**	**NDI**	-	-	-	-
7	**DMN**	**NDI**	5.7	-1.03	-10.68	-21.52

[a] Average value of three experiments

A self-association constant of 44 M^{-1} was measured for **1** at 298 K, which increases with temperature. Its polymer **2** registered self-association constant of 10^4 magnitude. These interactions may be due to offset π-stack geometry modulated by quadrupole interactions, which is favored entropically. This observation is consistent with Hunter and co-workers model for similar systems.[5] The strong CT complex observed for monomers of **NDI** and **PY** in 1:1 ratio may be due to identical molecular geometry, harmonious electron-rich electron-deficient surfaces (Figure 4.2), shape and molecular symmetry which allow them to orient better, thus beef-up the earlier findings of Kato et al. and our group. These interactions are favored enthalpically but decrease steadily with temperature as result of distortion of their orientation. In the case of **BAP**, the extra ring on the pyrene core alters the FMO symmetry, size and shape significantly and hence, affects its interaction with **NDI** under variable temperatures. Although **BAP** lacks comparable molecular geometry and symmetry as **PY**, at low temperature establishes favourable stacking alignment with **NDI** and consequently, gave a relatively high K_A (Table 4.2). This stacking organization is probably dropped sharply with increasing temperature, connoting prominent role of orientation in the formation of D-A CT process. The centrosymmetric and large π-surface area of **PERY** offer several possible orientations to interact with **NDI**, which translated into the high CT interactions observed for their complex. Computational analysis reveals that both **PY** and **DAP** have preserved FMO features; symmetries, shapes, sizes and π-areas. However, their electrostatic potential maps (Figure 4.2) clearly show that electrons are delocalized on the planar surface of **PY** but are localized on the diaza edges of **DAP** creating electron deficient planar surface on **DAP**. This difference in their planar electron distribution probably

mirrored into high in **PY** and undetectable in **DAP** CT interactions with **NDI**. For other donors with electron density in-phase as **PY**, inspection of the FMO shows lack of similar degree of harmony including low energy difference, HOMO symmetry, shape, size and area to match with **NDI**. The poor matching of geometry and symmetry of **CHR** with that of **NDI** did not facilitate strong CT interactions with **NDI**, though it possesses a relatively large π-area. Similar reasons may account for the low association constants in the case of **DMN-NDI** complex. The association constant obtained for **DMN-NDI** complex is however in good agreement with Iversion et al report.[86]

4.4 Effects of Switching from C_2 - to C_3 -Symmetric Molecules

Table 4.3 Thermodynamic profiles of C_2 and C_3 symmetric molecules.

Entry	Donor	Acceptor	$K_A(M^{-1})$[a]	ΔG(kcal/mol)	ΔH(kJ/mol)	ΔS(J/mol·K)
1	TPH	NDI	5.29	-0.96	39.28	145.25
2	PY	MTI	28.05	-1.98	-22.76	-48.64
3	TPH	MTI	26.40	-1.96	-27.81	-65.87
4	DMN	MTI	15.91	-1.63	17.12	80.33

[a] Average value of three experiments

Switching from a C_2-symmetry, two-electron-accepting diimides **1** to C_3-symmetry three-electron-accepting triimides **3** with the same donor (**PY**) led to significant rise in interactions between D-A pairs. For a 1:1 complex, the demand for electrons by **MTI** over **NDI** in **PY- MTI** system resulted in three fold increase in K_A. This interaction is enthalpically driven and decreases with temperature. This implies that increasing the symmetry, area and acceptability of the acceptor (**MTI**) enhance its association with a donor possibly through electrostatic complementarity and dispersion interactions initiated by the acceptor with a donor.

The **DMN-MTI** complex yielded K_A of 15.91 M^{-1} at 298 K, which increases with temperature and is entropically favored. This suggests that in addition to the rise in demand for electrons by **MTI**, **DMN** can also adopt different conformations while interacting with **MTI** such that at any point the electron difficient edges of the **DMN** stacked to the electron rich edges of the **MTI** posing extra stability for the interactions. This notion is consistent with the torsional motion of substituents on dimethylnaphthalene derivative reported by Wilson.[95] The magnitude of the association contant doubled from **DMN** to **PY** with same acceptor **MTI**. This could possibly due to molecular geometry of aromatic core of **PY** that offers a better orientation with **MTI** than **DMN**.

The improved electron donating ability by **TPH** in **TPH-NDI** complex show a general increase of the K_A with temperature. Two constrasting trends were observed for CT constants at varying temperature for **PY** and **TPH** with **NDI**. For **PY-NDI** complex, K_A decreases from 9.6 M^{-1} to 6.8 M^{-1} within temperature range of 298 K to 320 K. **TPH-NDI** on one hand increases from 5.29 M^{-1} to 16.41 M^{-1} in the same range, which indicates that increase in electron density for the same acceptor initially results in strong repulsive forces due to quadrupole interactions (supported by second term in Salem-Kloppman equation and Hunter's model) as the dominant factor at relatively low temperature. The association constant however, increase with temperature as electronic repulsion between D-A is minimized probably through a rise in entropy. It is obvious that using donor and acceptor of equivalent and higher electron donating and accepting abilities and symmetries improved the charge-transfer process as seen in the case of **TPH-MTI** complex over **PY-NDI** complex (Table 4.3).

4.5 Impact of Integrating Sandwich Molecular Constructs

Table 4.4 Thermodynamic profile of monomer-polymer molecular systems.

Entry	Donor	Acceptor	$K_A(M^{-1})^a$	ΔG(kcal/mol)	ΔH(kJ/mol)	ΔS(J/mol·K)
1	**pNDI(25mer)**	**pNDI(25mer)**	$8.4x10^4$	-6.66	-44.60	-56.30
2	**CHR**	**pNDI(25mer)**	34.89	-2.11	-20.43	-39.00
3	**DAP**	**pNDI(25mer)**	32.40	-2.10	-60.44	-173.81
4	**DMN**	**pNDI(25mer)**	10.40	-1.41	-26.62	-69.54

[a] Average value of three experiments

In sandwich molecular systems (monomer-polymer complexes), improved interactions of **pNDI** with donors such as **CHR**, **DMN** and **DAP** were observed. For the complexes of **CHR**- and **DMN**- with **pNDI**, the K_A increases by approximately six and two fold respectively, compare to their corresponding monomer pairs due to enhance molecular alignment during charge transfer formation. The location of electron density on the **DAP** produce detectable CT interaction in 1:1 ratio of **DAP-pNDI** complex, on exposer to suitable morphological orientation with acceptor polymer. The marked upfield shift of the aromatic protons of **pNDI** in complexes with **PY**, **PERY** and **BAP** makes it almost impossible to measure the CT constants. The shifting **pNDI** aromatic protons are completely masked by those of respective donors, and hence remain invisible in the ^1H NMR overlaid spectra (Figure 4.4).

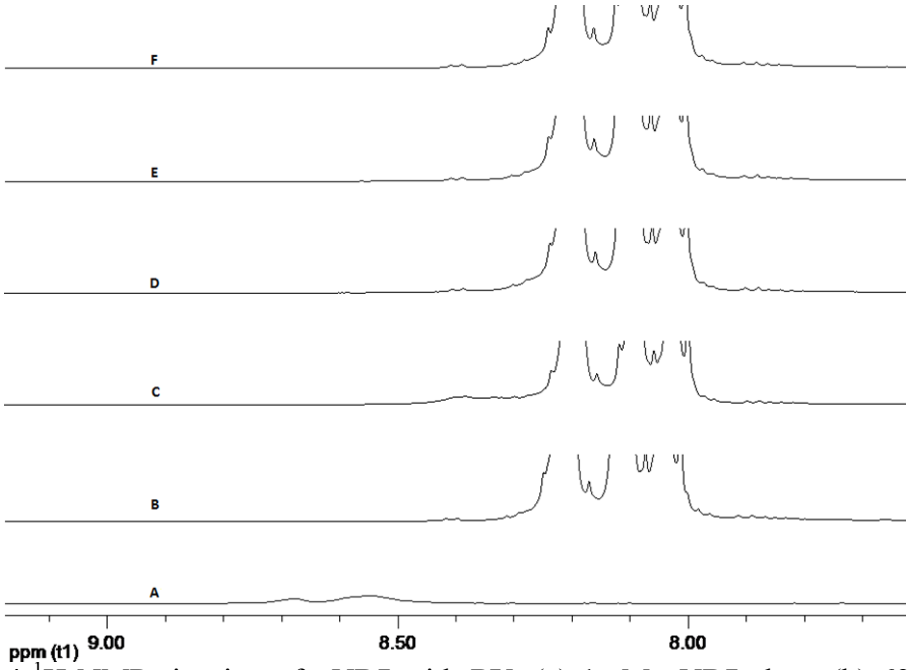

Figure 4.4 ^{1}H NMR titration of **pNDI** with **PY**; (a) 1mM **pNDI** alone (b) 63 mM **PY** alone, 1mM **pNDI** in (c) 10.5 mM **PY** (d) 18.0 mM **PY** (e) 23.6 mM **PY** (f) 28.0 mM **PY** @ 25°C. The aromatic protons of the **pNDI** cannot be seen in the spectra.

Though the shift in aromatic protons of **pNDI** demonstrates strong interactions with **PY**, **PERY**, and **BAP** in each case, the magnitude of these interactions cannot be readily quantified with the NMR technique, thus our resort to optical methods.

4.6 Steady State Emission and lifetime studies: K_{sv} and K_D

Table 4.5 Stern-Volmer (K_{sv}) and dynamic quenching (K_D) constants for **PY- pNDI (25mer)** complex.

Temperature (K)	K_{sv} (M^{-1})[a]	K_D(M^{-1})[a]
298	$7.9x10^4$	$1.1x10^3$
305	$7.5\ x10^4$	$1.3\ x10^3$
313	$6.7\ x10^4$	$1.0\ x10^4$
316	$6.6\ x10^4$	$1.0\ x10^4$

[a] Average of three experimental data

In a bid to quantify strong π-interactions of **PY**, **PERY** and **BAP** with **pNDI** observed in ^{1}H-NMR experiment, Stern-Volmer constant for both static and dynamic quenching was determined for **PY-pNDI** at varying temperatures.

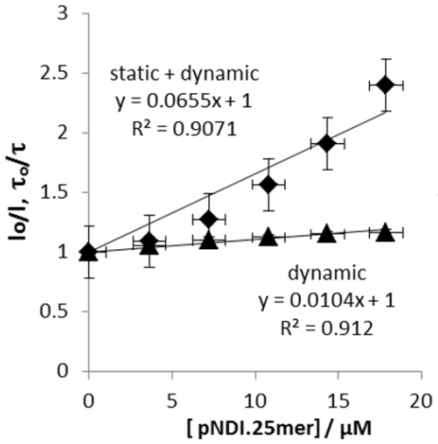

$$\frac{I^{\circ}}{I} = 1 + Ksv \cdot [Q]$$

Figure 4.5 Stern-Volmer plot for emission quenching and fluorescence lifetime decrease of **PY** on addition of **pNDI** (**25mer**) at 316 K. Error bars show s.e.m.

It can be inferred from this experiment (Table 4.5) that dynamic quenching significantly contributes to the interactions for monomer-polymer system. Due to the close overlap of the excitation wavelenghts of **PERY**- and **BAP**- with **pNDI**, similar experiments for these complexes proved futile as fluorescence enhancement occured until a high quencher concentration (700 µM of acceptor) before quenching is seen.

4.7 UV-visible dilution method: $K_{A'static}$

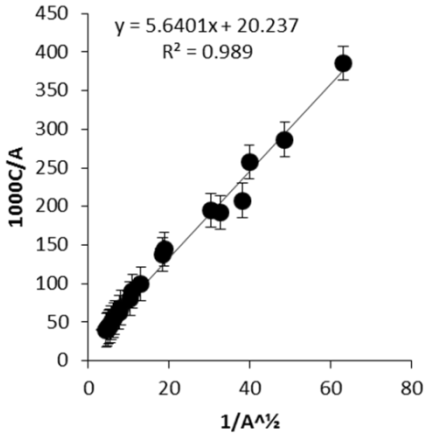

$$\frac{c}{A} = \left(\frac{1}{Ka \cdot \varepsilon \cdot l}\right)^{½} \cdot \frac{1}{A^{½}} + \frac{1}{\varepsilon \cdot l}$$

$$Ka = \frac{y_o}{\alpha\text{^}2}$$

Figure 4.6 Plot of d*A vs* $1/A^{½}$ for 1:1 mixture of each donor-acceptor pair. Each experiment consists of at least eleven data points ± s.e.m.

The K_As obtained from the UV-visible dilution titration plots [96] are summarized in Table 4.6. From the Figure 4.6 and Table 4.6 two distinct deductions can be made for the monomer pairs.

Table 4.6 Association constant and the corresponding wavelength at which CT occurred for donor-acceptor pairs.

Entry	Donor	Acceptor	$K_A(M^{-1})$[a]	λ_{CT} (nm)
1	**PY**	**NDI**	186.45	525
2	**PERY**	**NDI**	54.12	600
3	**BAP**	**NDI**	89.50	565
4	**PY**	**pNDI(25mer)**	636.17	525
5	**PERY**	**pNDI(25mer)**	70.34	600
6	**BAP**	**pNDI(25mer)**	30.00	565

[a] Average of three independent experimental data

First, high K_A observed for **PY**-**NDI** buttress the findings our group and Kato et al made earlier on. This indicates that besides frontier molecular orbitals congruency that contribute towards strong CT formation, molecular geometry, symmetry and area play decisive role on orientation of donors with acceptors at a long or short range and consequently, the strength of charge transfer. The presence of extra ring fused to pyrene in the case of **BAP** alters its orientation with **NDI**, which is remarked in approximately two-fold decrease in the CT constant at wavelength of 565 nm compared to that for **PY**-**NDI**. The **PERY**-**NDI** yielded K_A of 54.12 M^{-1}at 600 nm, though significantly high in magnitude represents the lowest with respect to values obtained for **PY** and **BAP** (Table 4.6). This suggests that in addition to centrosymmetry couple with large area of **PERY**, its static process of interaction with **NDI** is governed by other factors including a favorable orientation with acceptor molecule. Second, monitoring the wavelength with absorbance at which charge transfer occurred for each complex, and plotting *dA* against $1/A^{½}$, the highest K_A derived was 186.45 M^{-1} at 525 nm, which demonstrates that strong

charge transfer formation is concomitantly accompanied with large degree of energy. Based on similar procedure, moderate (89.5 M^{-1}) at 565 nm and least charge transfer constant (54.12 M^{-1}) at 600 nm were derived at moderate and least energies respectively. These signify the need for molecules involve in CT complex to exhibit high molar absorptivity in order to absorb sufficient photon energy to expedite single step electron transfer process.

The amplification of compatible symmetry, area and molecular alignment for **PY-pNDI** sandwich systems approximately quadruple the high charge transfer constant obtained for monomer pairs. Contrast to the improve CT constant measured for **PERY-pNDI** mainly due to better orientation offered by acceptor polymer, the K_A for **BAP-pNDI** decreases nearly three times due probably to minimum π-area contacts. The reduce area necessary for charge transfer interaction may arise from distorted molecular orientation. It is also envisage that increasing the acceptor polymer chain length has potential to enhance charge transfer process with **PY** and **PERY** but may lessen the extent of CT interaction for **BAP**.

Although a good correlation is observed in the data from both ^{1}H NMR experiment and UV-vis dilution method, the discrepancy found in the magnitude of the association constants may be ascribed to first, the different time scale of measurements. The ^{1}H NMR averages charge transfer interactions on 10^{-3} sec time-scale, which may not accurately account for molecular interactions faster than this scale. This limitation is better address on 10^{-15} sec time scale of UV-vis dilution. Moreover, the possibility of dephasing due to double quantum coherences which are created and evolved on the ms time-scale in NMR experiments may adversely represent the interactions of two

molecules beyond ~5 Å from each other.[97] The use of variant temperature in NMR has the tendency of widening the stacking angle and intermolecular distances between D and A molecules due to entropy effect and hence, the charge transferring process.

4.8 Conclusion

We have investigated the effects of molecular geometry, features of FMO and energy on the strength of CT formed by series of donor-acceptor complexes. A high association constant was determined for **PY**-**NDI** complex in all the techniques used. Not only does this confirm our earlier report but projects **PY** and **NDI** as potential molecules for single-step electron transfer without structure modifications. Inspection of the FMOs of these molecules reveals a close matching of the orbital size, shape, area, energy and symmetry of **PY** with **NDI** may be driving these interactions. Unlike **PY**, the strength of CT form with **NDI** depends on the orientation **PERY** presents despite its large area and centrosymmetry, which is evident in the UV-vis studies. **BAP** attains a better orientation with **NDI** to form strong CT complex at low temperatures, however, the interactions are weaken by the onset of molecular disorientation when temperature is increased. Interestingly, increasing the symmetry, area and acceptability of the acceptor (**MTI**) increase its association with a donor. This may be due to improve electrostatic complementarity and dispersion interactions initiated by the acceptor with a donor. The opposite trend is seen for a donor (**TPH**) of similar enhance structural features, which may stem from an increase electrostatic repulsion initiated by the donor. The UV-vis experiment suggests that contrast to potential enhance interactions that **PY** and **PERY** could produce with acceptor polymer of longer chain length, the interactions of **BAP** may be adversely affected. Employing polymer acceptor of longer chain length distorts

molecular orientation of **BAP** and therefore, its ability to yield high association with long chain polymer acceptor. Additionally, strong CT complexes were formed at relative low wavelength of absorption highlighting the importance of selecting molecules with high molar absorptivity. Future studies should focus on the use of transient absorption spectroscopy to investigate the time scale and the extent of free charge generated by each CT complex.

In summary, determination of charge transfer constants between D and A molecules show that in addition to remarkable high molar absorptivity necessary for single-step charge transfer from D to A FMO, factors including the shape, size, π-area, symmetry, energy gap between $HOMO_D$-$LUMO_A$, and the accepting capability of the acceptor predominantly dictate the directionality and thus, extent of CT form by each complex.

4.9 Experimental Section

4.10 Synthesis

A modified procedure reported by Rotello et al[7] was used to synthesize monomers **1** and **3** in scheme 1. The characterization of **NDI** has been reported by Icli et al. [98] The cooled dry crude product of **MTI** was dissolved in small amount of CH_2Cl_2 (about 5mL), and purified on silica packed column using DCM/hexane in the ratio of 4:1 by v/v, as eluent to give 40% yield of creamy white product. **3:** ^{1}H NMR (400 MHz, $CDCl_3$) δ: 3.9 (t, J = 7 Hz, 6H) 1.7 (m, 9H) 0.99 (m, 18H) ppm. ^{13}C (400 MHz, $CDCl_3$) δ: 163, 134, 39, 38, 26, 23 ppm. ES-TOF MS calcd for $C_{27}H_{33}N_3O_6$ (M^+) 495.24, found 518.2 ($[M + Na]^+$, 100%).

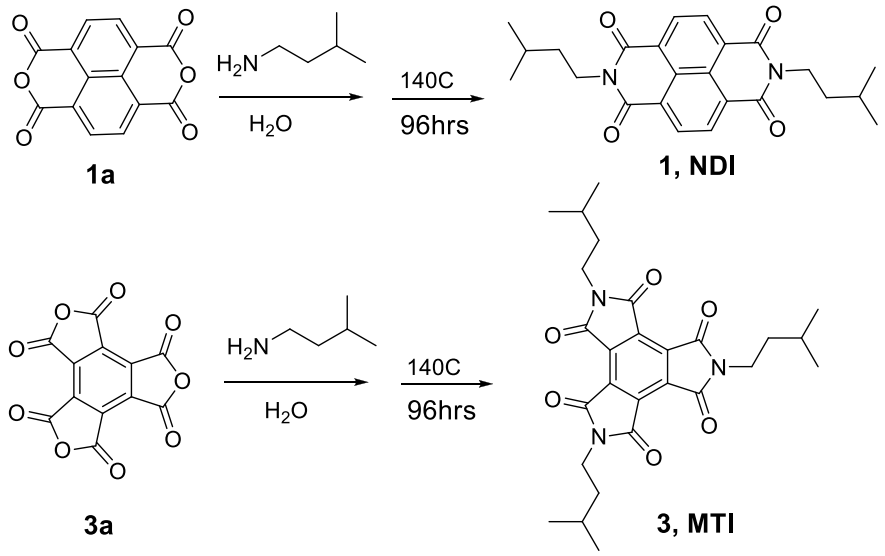

Scheme 1: Synthesis of **NDI** and **MTI** monomers.

Monomer **8** was prepared and characterized according to procedure reported by Cejas et al.[99]

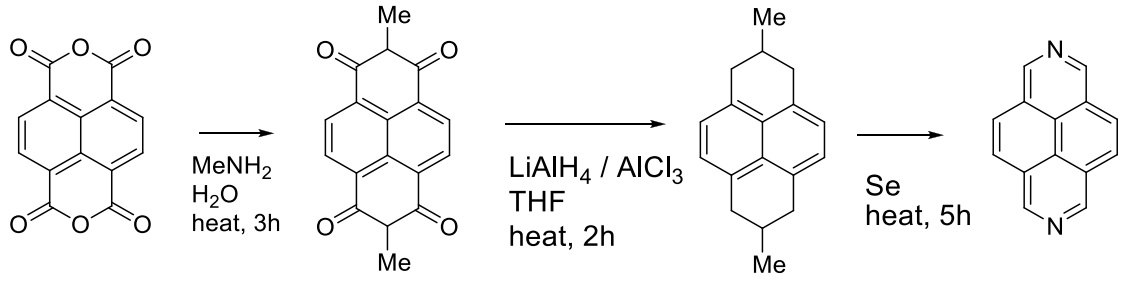

Scheme 2: Synthesis of **DAP** monomer.

Compound **9** was prepared using a modified synthetic procedure reported by Suhrit Ghosh et al.[100] The crude product was purified using column chromatography with hexane/DCM (2:3) eluent on silica packing as shown in the scheme 3. It was characterized as described in the same report.

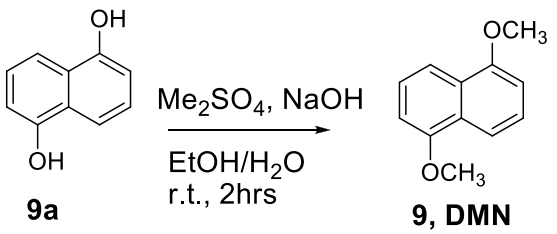

Scheme 3: Synthesis of **DMN** monomer.

The acceptor polymer **2** was synthesized by reacting **2c** (250 mg, 0.4630 mmol) with third generation Grubb's catalyst (0.01852 mmol) according to the procedure described by Kumar et al.[88] **2:** ^{1}H NMR (400 MHz, $CDCl_3$) δ: 0.9-1.1 (5.8H, s) 1.5-1.6 (6.7H, s) 1.9-2.2 (2.9H, br) 2.9-3.1 (3.1H, br, d) 3.3-3.6 (3.1H, br, t) 3.9-4.1 (3.9H, br) 5.1-5.5 (1.2H, br, s) 5.6-5.8 (1H, br, t) 8.5-8.7 (4H, br, d) ppm

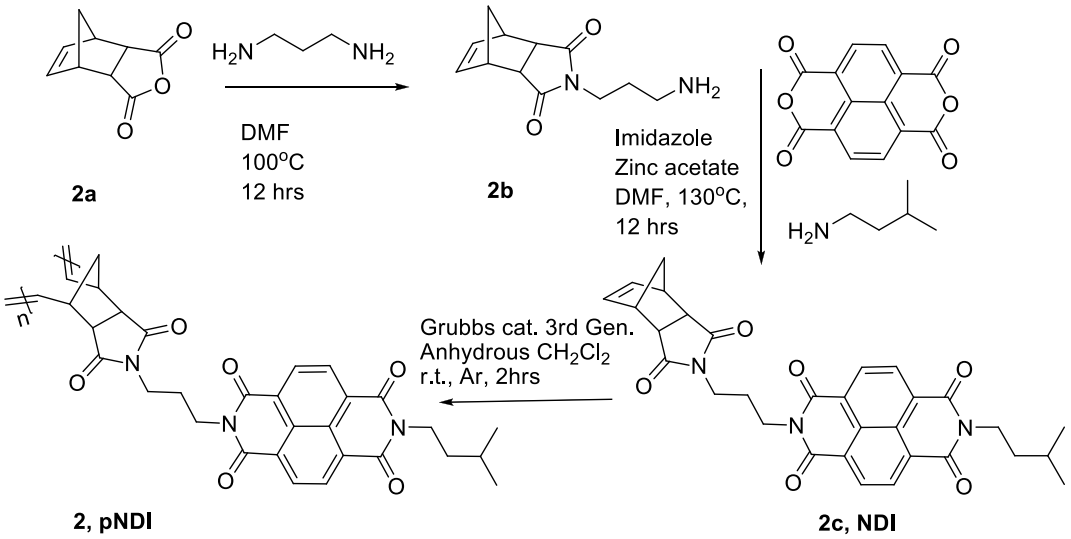

Scheme 4: Synthesis of polymer of **NDI** (**25mer**).

Monomers **4**, **5**, **6**, **7** and **10** were purchased from sigma Aldrich.

4.11 ^{1}H NMR Spectroscopy

Most acceptors have the propensity to self-associate,[86] 20 mM stock solution of **1** and **3** were prepared in $CDCl_3$. From these stocks several low concentrations of **1** and **3**

were prepared. Aliquots (700 μL) of each solution were transferred to clean and dry NMR sample tube. The aromatic signals of each acceptor were monitored with concentration using TMS reference. This provided information on the minimum concentration of each acceptor sensitive to the NMR instrument. Using method reported by Foster et al.,[101] the charge transfer constant of each D-A pair is determined by preparing series solutions consisting of variable concentrations of D and fix concentrations of A while ensuring that [D]>> [A] or vice versa. The ^{1}H NMR for each D-A pair is acquired on Bruker 400MHz after mixing for 5 - 10 min at temperature range of 298-320 K. The K_As obtain at specific temperatures are subjected to Van't Hoff's plot to obtain the ΔS and ΔH. The stoichiometry of each complex is determined by the procedure described by the Hirose[102] and data treated with Job's plot.

4.12 Steady state Emission and Absorption Spectroscopy

Steady state fluorescence and life time quenching were carried out on pyrene and polymer **NDI** (**25mer**) at temperatures of 298-316 K. 100 μM donor solution solution was sequentially quenched by micromolar (μM) additions of **pNDI** (**25mer**) in $CHCl_3$ at a known temperature. Lifetime quenching analysis was carried out on ISS frequency domain spectrometer Chrono FD with laser excitation and emission wavelengths of 280 nm and 370 nm respectively using 2,5-diphenyloxazole (PPO) scintillation grade(>99 % purity) in ethanol as a reference. Steady state quenching was performed on the same instrument at 310 nm excitation wavelength and 5 nm for both emission and excitation slits. Using path lengths of 1 cm for all experiments, the data from the decrease in fluorescence intensity and lifetime of thirteen titration points were analysed with Stern-Volmer plot.[103] Each experiment was repeated thrice.

The UV-vis. dilution was carried out by incremental mixing of equimolar amount of 11 mM each of D and A for pair D-A in $CHCl_3$ at 20 ºC. Their absorbance (at λ_{max}) was measured for eleven different concentrations in the range of 10^{-5} -10^{-3} M. The K_A was determined from linear plot of c/A with $A^{-1/2}$ based on Stoddard report.[96] The K_A for each donor-acceptor pair is the results from three independent measurements.

4.13 Computational Method

All calculations were performed with Spartan '08 software. Optimized geometry, area and energy of each molecule were calculated with DFT with B3LYP functional at the 6-31G* level in the gas phase.

References

[1] Sinkeldam, R. W.; Greco, N. J.; Tor, Y.,*Chem. Rev.* **2010,** *110*, 2579-2619.

[2] Giepmans, B. N. G.; Adams, S. R.; Ellisman, M. H.; Tsien, R. Y.,*Science* **2006,** *312*, 217-224.

[3] Warman, J. M.; de Haas, M. P.; Dicker, G.; Grozema, F. C.; Piris, J.; Debije, M. G.,*Chem. Mater.* **2004,** *16*, 4600-4609.

[4] Hoeben, F. J. M.; Jonkheijm, P.; Meijer, E. W.; Schenning, A. P. H. J.,*Chem. Rev.* **2005,** *105*, 1491-1546.

[5] Hunter, C. A.; Sanders, J. K. M.,*J. Am. Chem. Soc.* **1990,** *112*, 5525-5534.

[6] Nunzi, J.-M.,*C. R. Physique* **2002,** *3*, 523-542.

[7] Carroll, J. B.; Gray, M.; McMenimen, K. A.; Hamilton, D. G.; Rotello, V. M.,*Org. Lett.* **2003,** *5*, 3177-3180.

[8] Schmidt-Mende, L.; Fechtenkotter, A.; Mullen, K.; Moons, E.; Friend, R. H.; MacKenzie, J. D.,*Science* **2001,** *293*, 1119-1122.

[9] Gunes, S.; Neugebauer, H.; Sariciftci, N. S.,*Chem. Rev.* **2007,** *107*, 1324-1338.

[10] Valeur, B., *Molecular Fluorescence; "principles and applications"* 1st ed.; 2002.

[11] Singh, A.; Yip, W. T.; Halterman, R. L.,*Org. lett.* **2012,** *14*, 4046-4049.

[12] Tsien, R. Y.,*Annu. Rev. Neurosci.* **1989,** *12*, 227-253.

[13] Thomas, S. W.; Joly, G. D.; Swager, T. M.,*Chem. Rev.* **2007,** *107*, 1339-1386.

[14] Sinkeldam, R. W.; Marcus, P.; Uchenik, D.; Tor, Y.,*Chemphyschem* **2011,** *12*, 2260-2265.

[15] Disney, M. D.; Zheng, J.; Swager, T. M.; Seeberger, P. H.,*J. Am. Chem. Soc.* **2004,** *126*, 13343-13346.

[16] Raymond, S. B.; Skoch, J.; Hills, I. D.; Nesterov, E. E.; Swager, T. M.; Bacskai, B. J.,*Eur. J. Nucl. Med. Mol. Imaging* **2008,** *35*, S93-8.

[17] Grimme, S.,*Angew. Chem. Int. Ed.* **2008,** *47*, 3430-3434.

[18] Hunter, C. A.; Lawson, K. R.; Perkins, J.; Urch, C. J.,*J. Chem. Soc. Perk. Trans. 2* **2001**, 651-669.

[19] Birks, J. B.; Christophorou, L. G.,*Nature* **1963,** *197*, 1064-&.

[20] Clarke, T. M.; Durrant, J. R.,*Chem. Rev.* **2010,** *110*, 6736-6767.

[21] Muntwiler, M.; Yang, Q.; Tisdale, W. A.; Zhu, X. Y.,*Phys. Rev. Lett.* **2008,** *101*.

[22] Deibel, C.; Strobel, T.; Dyakonov, V.,*Adv. Mater.* **2010,** *22*, 4097-4111.

[23] Jelley, E. E.,*Nature* **1936,** *138*, 1009-1010.

[24] Jelley, E. E.,*Nature* **1937,** *139*, 631-632.

[25] Behera, G. B. B., P.K.; Mishra, B.K.,*J. Surf. Tech.* **2007,** *23*, 1-31.

[26] Coluccini, C.; Sharma, A. K.; Caricato, M.; Sironi, A.; Cariati, E.; Righetto, S.; Tordin, E.; Botta, C.; Forni, A.; Pasini, D.,*PhysChemChemPhys* **2013,** *15*, 1666-74.

[27] de Silva, A. P.; Gunaratne, H. Q. N.; Gunnlaugsson, T.; Huxley, A. J. M.; McCoy, C. P.; Rademacher, J. T.; Rice, T. E.,*Chem. Rev.* **1997,** *97*, 1515-1566.

[28] Marini, A.; Munoz-Losa, A.; Biancardi, A.; Mennucci, B.,*J. Phys. Chem. B* **2010,** *114*, 17128-17135.

[29] Baraldi, I.; Brancolini, G.; Momicchioli, F.; Ponterini, G.; Vanossi, D.,*Chem. Phys.* **2003,** *288*, 309-325.

[30] Zhang, Z.; Wallace, M. B.; Feng, J.; Stafford, J. A.; Skene, R. J.; Shi, L.; Lee, B.; Aertgeerts, K.; Jennings, A.; Xu, R.; Kassel, D. B.; Kaldor, S. W.; Navre, M.; Webb, D. R.; Gwaltney, S. L.,*J. Med. Chem.* **2011,** *54*, 510-24.

[31] Zhu, Y. F.; Guo, Z. Q.; Gross, T. D.; Gao, Y. H.; Connors, P. J.; Struthers, R. S.; Xie, Q.; Tucci, F. C.; Reinhart, G. J.; Wu, D. P.; Saunders, J.; Chen, C.,*J. Med. Chem.* **2003,** *46*, 1769-1772.

[32] Winkley, M. W.; Robins, R. K.,*J. Org. Chem.* **1969,** *34*, 431-&.

[33] Wang, G.; Tam, R. C.; Gunic, E.; Du, J.; Bard, J.; Pai, B.,*J. Med. Chem.* **2000,** *43*, 2566-74.

[34] Shafer, C. M.; Lindvall, M.; Bellamacina, C.; Gesner, T. G.; Yabannavar, A.; Jia, W. P.; Lin, S.; Walter, A.,*Bioorg. Med. Chem. Lett.* **2008,** *18*, 4482-4485.

[35] Prasad, Y. R. R., K.K.; Shankarananth V.; Maulaali, S.C.; Kumar, G.S.S.P.; Reddy, K.N.,*J. Pharm. Res.* **2010,** *3*, 2291-2.

[36] Wilhelmsson, L. M.; Sandin, P.; Holmen, A.; Albinsson, B.; Lincoln, P.; Norden, B.,*J. Phys. Chem. B* **2003,** *107*, 9094-9101.

[37] Wu, H.; Chen, X. M.; Wan, Y.; Ye, L.; Xin, H. Q.; Xu, H. H.; Pang, L. L.; Ma, R.; Yue, C. H.,*J. Chem. Res.* **2008**, 711-714.

[38] Netzel, T. L.; Zhao, M.; Nafisi, K.; Headrick, J.; Sigman, M. S.; Eaton, B. E.,*J. Am. Chem. Soc.* **1995,** *117*, 9119-9128.

[39] Krueger, A. T.; Lu, H.; Lee, A. H.; Kool, E. T.,*Acc. Chem. Res.* **2007,** *40*, 141-50.

[40] Godde, F.; Toulme, J. J.; Moreau, S.,*Nucleic Acids Res.* **2000,** *28*, 2977-85.

[41] Shin, D.; Sinkeldam, R. W.; Tor, Y.,*J. Am. Chem. Soc.* **2011,** *133*, 14912-5.

[42] Wilson, J. N.; Kool, E. T.,*Org. Biomol. Chem.* **2006,** *4*, 4265-74.

[43] Tanpure, A. A.; Srivatsan, S. G.,*Chem. - Eur.* **2011,** *17*, 12820-7.

[44] Nishio, T.; Omote, Y.,*J. Chem. Soc. Perk. Trans 1* **1984**, 239-242.

[45] Dhuguru, J.; Gheewala, C.; Kumar, N. S.; Wilson, J. N.,*Org. Lett.* **2011,** *13*, 4188-91.

[46] Reichardt, C.,*Angew. Chem. Int. Ed.* **1979,** *18*, 98-110.

[47] Fahrni, C. J.; Henary, M. M.; VanDerveer, D. G.,*J. Phys. Chem. A* **2002,** *106*, 7655-7663.

[48] Jacques, P.; Graff, B.; Diemer, V.; Ay, E.; Chaumeil, H.; Carre, C.; Malval, J. P.,*Chem. Phys. Lett.* **2012,** *531*, 242-246.

[49] Muthuramu, K.; Ramamurthy, V.,*J. Photochem.* **1984,** *26*, 57-64.

[50] Hong, Y.; Lam, J. W.; Tang, B. Z.,*Chem. Commun.* **2009**, 4332-53.

[51] Berlman, I., *Handbook of Fluorescence Spectra of Aromatic Molecules*. 2nd ed.; Academic Press: New York, 1971.

[52] Apex2 Version 2.2-0 and SAINT+ Version 7.46A Bruker Analytical X-ray System, Inc.,: Madison, Wisconsin, USA, 2007.

[53] (a) Sheldrick, G. M.,*Acta Crystallogr. A* **2008,** *64*, 112-122; (b) Sheldrick, G. M. SHELXTL Version 6.1; Bruker Analytical X-ray Systems, Inc.: Madison, Wisconsin, USA., 2000.

[54] Revision A.1, F., M. J.; Trucks, G. W.; Schlegel, H. B.; Scuseria, G. E.; Robb, M. A.; Cheeseman, J. R.; Scalmani, G.; Barone, V.; Mennucci, B.; Petersson, G. A.; et al. Gaussian, Inc.,: Wallingford CT, , 2009.

[55] Lin, W. B.; Yitzchaik, S.; Lin, W. P.; Malik, A.; Durbin, M. K.; Richter, A. G.; Wong, G. K.; Dutta, P.; Marks, T. J.,*Angew. Chem. Int. Ed.* **1995,** *34*, 1497-1499.

[56] Yang, Z.; Aravazhi, S.; Schneider, A.; Seiler, P.; Jazbinsek, M.; Gunter, P.,*Adv. Funct. Mater.* **2005,** *15*, 1072-1076.

[57] Bussemer, B.; Dreiling, I.; Grummt, U. W.; Mohr, G. J.,*J. Photoch. Photobio. A* **2009,** *204*, 90-96.

[58] Shiraishi, Y.; Inoue, T.; Hirai, T.,*Langmuir* **2010,** *26*, 17505-17512.

[59] Kashida, H.; Sano, K.; Hara, Y.; Asanuma, H.,*Bioconjugate Chem.* **2009,** *20*, 258-265.

[60] Mitchell, H. A.; Weinshenker, D.,*Biochem. Pharmacol.* **2010,** *79*, 801-809.

[61] Tully, K.; Bolshakov, V. Y.,*Mol. Brain* **2010,** *3*.

[62] Hadrich, D.; Berthold, F.; Steckhan, E.; Bonisch, H.,*J. Med. Chem.* **1999,** *42*, 3101-8.

[63] Schwartz, J. W.; Blakely, R. D.; DeFelice, L. J.,*J. Biol. Chem.* **2003,** *278*, 9768-77.

[64] Brown, A. S.; Bernal, L. M.; Micotto, T. L.; Smith, E. L.; Wilson, J. N.,*Org. Biomol. Chem.* **2011,** *9*, 2142-8.

[65] Smith, E. L.; Brown, A. S.; Adjaye-Mensah, E.; Wilson, J. N.,*Org. Biomol. Chem.* **2012,** *10*, 1493-6.

[66] Brooker, L. G. S.; Keyes, G. H.; Heseltine, D. W.,*J. Am. Chem. Soc.* **1951,** *73*, 5350-5356.

[67] Murugan, N. A.; Kongsted, J.; Rinkevicius, Z.; Aidas, K.; Agren, H.,*J. Phys. Chem. B* **2010,** *114*, 13349-13357.

[68] Phanstiel, O. A., J. J. ,*RSC Drug Discovery Ser.* **2012,** *17*, 162-190.

[69] Solntsev, K. M.; McGrier, P. L.; Fahrni, C. J.; Tolbert, L. M.; Bunz, U. H.,*Org. Lett.* **2008,** *10*, 2429-32.

[70] Dominguez, M.; Rezende, M. C.,*J. Phys. Org. Chem.* **2010,** *23*, 156-170.

[71] Jacques, P.,*J. Phys. Chem.* **1986,** *90*, 5535-5539.

[72] Gleicher, G. J.; Church, D. F.; Arnold, J. C.,*J. Am. Chem. Soc.* **1974,** *96*, 2403-2409.

[73] Menting, K. H.; Eichel, W.; Riemenschneider, K.; Schmand, H. L. K.; Boldt, P.,*J. Org. Chem.* **1983,** *48*, 2814-2820.

[74] Lippert, E. Z.,*Elektrochem.* **1957,** *61*, 962-975.

[75] Yanai, T.; Tew, D. P.; Handy, N. C.,*Chem. Phys. Lett.* **2004,** *393*, 51-57.

[76] Marenich, A. V.; Cramer, C. J.; Truhlar, D. G.,*J. Phys. Chem. B* **2009,** *113*, 4538-4543.

[77] Zucchero, A. J.; McGrier, P. L.; Bunz, U. H. F.,*Acc. Chem. Res.* **2010,** *43*, 397-408.

[78] Mukherjee, S.; Chattopadhyay, A.; Samanta, A.; Soujanya, T.,*J. Phys. Chem.* **1994,** *98*, 2809-2812.

[79] Lehn, J. M.,*Angew. Chem. Int. Ed.* **1990,** *29*, 1304-1319.

[80] Cheon, J. D.; Mutai, T.; Araki, K.,*Org. Biomol. Chem.* **2007,** *5*, 2762-2766.

[81] Burley, S. K.; Petsko, G. A.,*Science* **1985,** *229*, 23-28.

[82] Lokey, R. S.; Iverson, B. L.,*Nature* **1995,** *375*, 303-305.

[83] Nelson, J.,*Science* **2001,** *293*, 1059-1060.

[84] Berggren, M.; Inganas, O.; Gustafsson, G.; Rasmusson, J.; Andersson, M. R.; Hjertberg, T.; Wennerstrom, O.,*Nature* **1994,** *372*, 444-446.

[85] Ortholand, J. Y.; Slawin, A. M. Z.; Spencer, N.; Stoddart, J. F.; Williams, D. J.,*Angew. Chem. Int. Ed.* **1989,** *28*, 1394-1395.

[86] Cubberley, M. S.; Iverson, B. L.,*J. Am. Chem. Soc.* **2001,** *123*, 7560-7563.

[87] Woodward, R. B.; Hoffmann, R.,*Angew. Chem. Int. Ed.* **1969,** *8*, 781.

[88] Kumar, N. S.; Gujrati, M. D.; Wilson, J. N.,*Chem. Commun.* **2010,** *46*, 5464-6.

[89] Gujrati, M. D.; Kumar, N. S. S.; Brown, A. S.; Captain, B.; Wilson, J. N.,*Langmuir* **2011,** *27*, 6554-6558.

[90] Fleming, I., *Molecular Orbital and Organic Chemical reactions*.

[91] Kato, S.; Matsumoto, T.; Ideta, K.; Shimasaki, T.; Goto, K.; Shinmyozu, T.,*J. Org. Chem.* **2006,** *71*, 4723-4733.

[92] Handbook on Molecular Switches. B.L., F., Ed. 2001; pp. 1-30.

[93] Mozer, A. J. S., N.S.,*C. R. Chimie* **2006,** *9*, 568-577.

[94] Chudek, J. A.; Foster, R.; Twiselton, D. R.,*J. Chem. Soc. Perk. Trans. 2* **1983**, 1385-1389.

[95] Wilson, C. C.,*Chem. Phys. Lett.* **2002,** *362*, 249-254.

[96] Nielsen, M. B.; Jeppesen, J. O.; Lau, J.; Lomholt, C.; Damgaard, D.; Jacobsen, J. P.; Becher, J.; Stoddart, J. F.,*J. Org. Chem.* **2001,** *66*, 3559.

[97] Marcon, V.; Breiby, D. W.; Pisula, W.; Dahl, J.; Kirkpatrick, J.; Patwardhan, S.; Grozema, F.; Andrienko, D.,*J. Am. Chem. Soc.* **2009,** *131*, 11426-11432.

[98] Erten, S.; Alp, S.; Icli, S.,*J. Photoch. Photobio. A* **2005,** *175*, 214-220.

[99] Cejas, M. A.; Raymo, F. M.,*Langmuir* **2005,** *21*, 5795-5802.

[100] Ghosh, S.; Ramakrishnan, S.,*Macromolecules* **2005,** *38*, 676-686.

[101] Foster, R.; Fyfe, C. A.; Foreman, M. I.,*Chem. Commun.* **1967**, 913.

[102] Hirose, K.,*J. Incl. Phenom. Macro.* **2001,** *39*, 193-209.

[103] Andrew, T. L.; Swager, T. M.,*J. Polym. Sci. Pol. Phys.* **2011,** *49*, 476-498.